UNIVERSITY OF CALIFORNIA

Santa Barbara

Contribution of chromophoric dissolved organic matter to attenuation of
ultraviolet radiation in three contrasting coastal areas

A Dissertation submitted in partial satisfaction
of the requirements for the degree of

Doctor of Philosophy

in

Marine Science

by

Karen Whitney Patterson

Committee in charge:

Professor Raymond C. Smith, Chairperson

Professor Libe Washburn

Professor Tommy Dickey

March 2000

The dissertation of Karen Whitney Patterson is approved

Tommy D. Dickey

Libe Washburn

Raymond C Smith

Committee Chairperson

March 2000

ACKNOWLEDGEMENTS

VITA

December 13, 1971 – Born – Baltimore, Maryland

1991-92 – Laboratory Assistant, Department of Geography, Salisbury State
University

1992 – University of Maryland Sea Grant College Remote Sensing of the
Oceans Summer Fellow, Atmospheric Chemistry and Dynamics
Branch, NASA/Goddard Space Flight Center

1992 – B.S., Mathematics and Geography, Salisbury State University

1993 – Universities Space Research Association - Graduate Student
Summer Program Fellow, Atmospheric Chemistry and Dynamics
Branch, NASA/Goddard Space Flight Center

1993-96 – Graduate Student Researcher, Institute for Computational Earth
Systems Science, University of California – Santa Barbara

1994-96 – Teaching Assistant, Department of Geography, University of
California – Santa Barbara

1996 – M.A., Geography, University of California – Santa Barbara

1996-99 – Environmental Protection Agency, Science To Achieve Results
Fellow, University of California, Santa Barbara

1998-99 – Environmental Protection Agency, National Network for
Environmental Monitoring Systems Fellow, National Environmental
Research Laboratory/Ecosystems Research Division

1999-2000 – Graduate Student Researcher, Institute for Computational
Earth Systems Science, University of California – Santa Barbara

PUBLICATIONS

Patterson, K.W., R.C. Smith, P.L. Handley. (1996) Palmer LTER: Open water PUV albedo measurements. *Antarctic Journal U.S. - 1996 Review*. 170 – 171.

Patterson, K.W., R.C. Smith, C.R. Booth. (1997) A method for removing a majority of the error in PUV attenuation coefficients due to spectral drift in response with depth in the water column. *Ocean Optics XIII*: Halifax, Nova Scotia, Canada, 22-25 October 1996. SPIE Volume 2963. Steven G. Ackleson and Robert Frouin editors. pp. 737 – 742.

Patterson, K.W. (1996) *Calculation of biologically effective UV dose rates for larval anchovies in the Southern California Bight using PUV data in combination with a simple high-spectral resolution model*. Master's Thesis. University of California, Santa Barbara.

Patterson, K.W. (1995) Attenuation in Kane'ohe Bay as interpreted from PUV profiles. In: *Ultraviolet Radiation and Coral Reefs*. D. Gulko and P.L. Jokiel (eds.), HIMB Tech. Report #41.UNIHI-Sea Grant-CR-95-03. 37 – 41.

Peterson, P.J.M., R.C. Smith, K.W. Patterson, P.L. Jokiel. (1995) A Biological Weighting Function for Phytoplankton Growth Inhibition. In: *Ultraviolet Radiation and Coral Reefs*. D. Gulko & P.L. Jokiel (eds.), HIMB Tech. Report #41.UNIHI-Sea Grant-CR-95-03. 53 – 61.

FIELDS OF STUDY

Optical Oceanography – Ultraviolet radiation in coastal ecosystems
Professor Raymond C. Smith

ABSTRACT

Contribution of chromophoric dissolved organic matter to attenuation of
ultraviolet radiation in three contrasting coastal areas

by

Karen Whitney Patterson

Assessing the impact of ultraviolet (UV) radiation on marine
ecosystems has been a topic of concern due to observed decreases in
stratospheric ozone concentrations since the 1970's. The high energy
UVB (280-320nm) radiation is of particular interest since the potential for
ecologically significant photobiological and photochemical processes
generally increases with decreasing UV wavelength. Wavelengths shorter
than the UVB are not considered ecologically significant as the earth's
atmosphere eliminates these wavelengths. To study the impact of UV
radiation on marine ecosystems, one needs to accurately measure water
column UV radiation and to understand the variability in and controls of UV
in seawater. In coastal ecosystems, the water column UV radiation field is
somewhat more complex than in the open ocean due to terrestrial
influences, such as riverine input of humic substances.

The main goals of this work were (1) to develop a consistent
database of UV measurements in contrasting coastal regions and to
develop satellite-applicable algorithms for estimating seawater UV
attenuation, (2) to characterize UV spatial and temporal variability in each
region, and (3) to assess the role played by the highly UV-absorbing
dissolved compounds, known as chromophoric dissolved organic matter

(CDOM), in terms of its contribution to total UV attenuation and UV variability in each coastal region. The three coastal regions sampled during the period from September 1997 – March 1999 were: the productive upwelling ecosystem of the Santa Barbara Channel, the shallow tropical ecosystem of the lower Florida Keys; and the ice-driven ecosystem off the west Antarctic Peninsula. In each region, water samples were collected for spectrophotometric light absorption by CDOM along with water column profiles of broadband UV and visible solar radiation using a hybrid PRR/PUV instrument. Ultraviolet attenuation in surface waters correlated well with light attenuation at 412nm and the SeaWiFS-relevant remote sensing ratio of $R_{rs}(555nm)/R_{rs}(412nm)$. Spatial and temporal patterns in total UV attenuation and CDOM absorption were complex and could only be explained for specific events. The contribution of CDOM absorption to total UV attenuation varied widely within and among the regions sampled, but generally dominated UV attenuation at 305nm.

TABLE OF CONTENTS

List of Figures

List of Tables

1. INTRODUCTION

Documented decreases in stratospheric ozone since the 1970's (i.e. Dutsch and Staehlin, 1989; Herman *et al.*, 1996; McPeters *et al.*, 1996) have in recent decades spawned great interest in studying the possible effects of increased solar ultraviolet (UV) radiation on various organisms and ecosystems. The role that UV radiation plays in marine ecosystems is of particular concern (Häder *et al.*, 1995). The world's oceans cover approximately two-thirds of the earth and play a significant role in the earth's carbon budget; phytoplankton, living in sunlit surface waters are the main biological sink for atmospheric carbon dioxide in the ocean.

For discussion purposes, the ultraviolet spectrum is broken into three wavelength regions, UVA (320-400nm), UVB (280-320nm) and UVC (100-280nm). Ultraviolet-C wavelengths are virtually eliminated by the atmosphere and do not reach the earth's surface in ecologically significant quantities. Ozone is a major absorber of UVB radiation (Molina and Molina, 1986). Surface visible, UVA and UVB radiation can also be altered by cloud cover and some atmospheric aerosols.

As wavelength decreases from the UVA through the UVB, the energy per photon increases. The activity-provoking potential per photon for many photobiological and photochemical processes generally increases with decreasing wavelength as well. For biological processes, the activity-provoking potential per photon is generally expressed by means of an action spectrum or biological weighting function (BWF), which expresses the relative response of an organism to photons of different wavelengths. A few examples of BWF's are plotted in Figure 1. In the marine environment, potential photobiological and photochemical processes include DNA damage (Setlow, 1974; Hunter *et al.*, 1981), phytoplankton

photoinhibition (Cullen *et al.*, 1992; Jones and Kok, 1966) and photochemical breakdown of chromophoric dissolved organic matter (CDOM) (Moran and Zepp, 1997; Kouassi and Zika, 1992), all three of which can have important implications for global carbon cycling and ecosystem community interactions (reviewed in Häder *et al.*, 1995; Zepp *et al.*, 1995; Häder and Worrest, 1991; Bothwell *et al.*, 1994).

In order to study the possible effects of changes in UV radiation on marine ecosystems, natural levels of and variability in water column UV need to be established. Describing the variability and controls of UV radiation in coastal waters proves a difficult task, especially over large areas and long time scales. Instrumentation for measuring water column UV varies widely in terms of sensor characteristics (i.e. bandwidth, counting photons versus measuring total energy), deployment capabilities and depth/time integrations at the time of data collection. In seawater, shorter UVB wavelengths are attenuated quickly while longer UVA wavelengths penetrate to much greater depths (Figure 2). Thus, small changes in instrument characteristics, such as bandwidth, can result in datasets collected with different types of instrumentation being incomparable.

Three contrasting coastal areas were chosen for studying natural variability of UV attenuation in surface waters from September, 1997 – March, 1999. Since obtaining comparable UV marine datasets for studies over large areas or time scales is extremely difficult, one of the main goals of this research was to develop globally applicable algorithms for estimating UV penetration through surface waters from more commonly measured water column parameters. Therefore, regions were chosen so as to maximize the variability in water column composition, physical characteristics and solar radiation environments.

2

The first study region was the Santa Barbara Channel, which is part of the high-productivity, cold-water California Current upwelling ecosystem. Issues concerning UV radiation in the Santa Barbara Channel and California Current ecosystems include the effects UV radiation have on primary productivity and the eggs and larvae of pelagic fish (Hunter *et al.*, 1981; Hunter *et al.*, 1982; Vetter *et al.*, 1999). The channel is a complex mixing pot, with colder northern waters entering through the west channel entrance, warmer southern waters entering through the southeast channel entrance and periodic upwelling events (Harms and Winant, 1998; Hendershott and Winant, 1996). The terrestrial influences on the ecosystem are seasonal with a large majority of the input of sediments and dissolved organic matter occurring during the rainy season, which occurs from November through March (National Weather Service – Santa Barbara climatology web page http://www.nwsla.noaa.gov/climate/sba/sbatex; Mertes *et al.*, 1998). As the rainy season ends, spring phytoplankton blooms are common, which are followed in summer and fall by periods of low concentrations of particulate matter (Venrick, 1998). Within the general annual cycles, interannual variability can be quite high as the Santa Barbara Channel is located in an area where El Niño – Southern Oscillation (ENSO) fluctuations can be pronounced (Pares-Sierra and O'Brien, 1989; Murphree and Reynolds, 1995; Lenarz *et al.*, 1995). The Santa Barbara Channel is also unique compared to the other study regions due to the existence of some of the world's most active natural oil seeps (Hornafius *et al.*, 1999), which are high UV absorbers (Klimkin, 1993).

The second region studied was the warm tropical coral reefs between Key West, Florida and the Dry Tortugas. Data were collected during an Environmental Protection Agency (EPA) project focused on assessing the effects of multiple stresses on coral reefs. While coral

bleaching is most often attributed to temperature (Goreau and Hayes, 1994), other water column variable changes, such as variations in nutrients, salinity, sedimentation, and UV radiation, can also affect the health and productivity of reef organisms (Hoegh-Guldberg and Smith, 1989; Lesser *et al*., 1990, Kinzie, 1993; Gleason and Wellington, 1993; Gleason, 1993). Since tropical reef organisms live in environments generally characterized by low climate variability compared other regions of the globe, they are often adapted to thrive in a more constrained niche environment. Thus, the potential exists for seemingly extreme or exaggerated responses by reef organisms for what might be considered a small change in an environmental variable, such as temperature (Goreau and Hayes, 1994), if that change occurs near the edge of the climatologically adapted range of the organism. However, organism and/or reef response to simultaneous changes in multiple environmental variables is much more difficult to predict as a change in one variable may diminish or compound the response due to changes in another environmental variable (Hughes and Connel, 1999; Porter *et al*., 1999). In general, tropical reef waters have been described as being optically clear and warm, with low amounts of nutrients and particulates in the water column. However, in the Florida Keys region, visible water clarity is not necessarily a good proxy for estimating water column UV attenuation, as will be discussed later. A unique characteristic of the Florida Keys region compared to the other two study regions is the bathymetric configuration of the area. To the north, there is a broad shallow shelf where depths are generally <20m extending from the Florida Everglades wetlands and waters are rich in UV-absorbing dissolved organic material, while to the south and west, waters are often more UV transparent, with depths increasing rapidly to >1000m.

The third region studied was the very cold waters of the west Antarctic Peninsula, which was unique in terms of terrestrial influence and the solar radiation environment. The Antarctic landmass is mostly ice covered with very little soil and plant material in comparison with the rest of the earth's landmasses. Other ice influences in this region include seasonal input of glacial flour and highly variable seasonal sea ice coverage. In fact, much of the ecosystem of the west Antarctic Peninsula is driven or significantly impacted by sea ice dynamics (Smith *et al.*, 1995). Sea ice and the solar radiation environment are probably the two dominant controls on Antarctic marine ecosystems. Due to Antarctica's global position, phytoplankton productivity is restricted mainly to the sunlit summer months of September – March. In addition, the UV-visible balance of solar radiation reaching the surface in the Antarctic is significantly altered in the spring months of September – December due to the Antarctic ozone hole (Lubin and Frederick, 1991; Smith *et al.*, 1992). While the main focus of this research is coastal environments, the coastal Antarctic waters sampled showed relatively low productivity and included open ocean characteristics, with stations extending over 200km offshore where water depths were sometimes >3000m.

With the development of the CZCS (Coastal Zone Color Scanner) and SeaWiFS (Sea-viewing Wide Field-of-view Sensor) satellite sensors came the standardization of instrumentation for measuring solar visible (400-700nm) radiation in the marine environment. To establish relationships between water column UV and the more commonly available water column visible measurements at SeaWiFS wavelengths, a hybrid PRR/PUV (Profiling Reflectance Radiometer/Profiling Ultraviolet Radiometer) instrument was used to collect over 280 casts of simultaneous profiles of in-water UV and visible radiation in the three study regions. An

additional advantage to using the hybrid PRR/PUV instrument was that the PRR measures both downwelling and upwelling radiation, from which SeaWiFS remote sensing reflectances could be calculated. While SeaWiFS satellite algorithms have been developed for estimating UV-absorbing CDOM in surface waters (Hoge *et al.*, 1995; Tassan, 1994), there is currently a lack of satellite-based algorithms for estimating the penetration of UV in surface waters. It is the net penetration of UV radiation through the water column that is of interest in studying many photobiological and photochemical processes occurring in marine ecosystems, not just the absorption of UV by a single component of seawater. From the PRR remote sensing reflectances, an algorithm was developed for estimating UV attenuation at PUV wavelengths in coastal waters from SeaWiFS satellite measurements.

The variability in water column UV can be better understood by independently measuring UV attenuation by the different components of seawater and identifying parameters controlling the variability in these substances. There are three main categories of substances contributing to the attenuation of solar UV and visible radiation in seawater (Figure 2). First, the seawater itself attenuates solar radiation in this range, though the magnitude of seawater absorption at UV wavelengths remains highly controversial, as will be discussed in Chapter 4. The second category is total particulate matter, which is often further divided into subcategories such as attenuation by phytoplankton and attenuation by non-living particulates, or detritus. The third category is dissolved organic matter, or more specifically, chromophoric (or colored) dissolved organic matter (CDOM). As wavelength decreases in the UV, CDOM absorption increases exponentially and absorption by CDOM (a_{CDOM}) often dominates over seawater and particulate attenuation at UVB wavelengths. For a

more complete discussion of the components contributing to the attenuation of UV radiation in seawater, the reader is referred to Kirk (1994a; 1994b).

Continuous UV-visible CDOM absorption spectra were measured from discrete water samples collected at approximately the same time and locations as the PRR/PUV casts in each of the study regions. In the literature, the shape of the UV-visible CDOM absorption spectrum is generally described by two parameters, the absorption value at a reference wavelength and the slope of an exponential curve fit: (Bricaud *et al.*, 1981):

$$a_{CDOM}(\lambda) = a_{CDOM}(\lambda_r)e^{-S(\lambda-\lambda_r)}$$

$$\lambda = \text{wavelength (nm)}$$

$$\lambda_r = \text{reference wavelength (nm)}$$

$$S = \text{slope parameter (nm}^{-1}\text{)}$$

While reported slope values range from $0.010 - 0.033\text{nm}^{-1}$ (Kirk, 1994b; Green and Blough, 1994; Vodacek *et al.*, 1997), a value of 0.014nm^{-1} is often used in optical ocean models (Baker and Smith, 1982; Tassan, 1994). However, analysis of hundreds of a_{CDOM} spectra show that the slope values for simple exponential curve fits are often highly dependent on the wavelength range used for the calculation and a simple exponential curve may not be sufficient to describe the UV a_{CDOM} spectrum. Since a_{CDOM} decreases nearly exponentially with increasing wavelength through the UV and visible, the wavelength dependence of the slope parameter could cause significant errors in optical ocean models of the UV part of the spectrum. Errors in the a_{CDOM} slope parameter would be of more minor concern for visible ocean optics models, as CDOM absorption generally contributes a small or negligible amount to total attenuation at visible wavelengths (Figure 2).

In estimating the ecological significance of UV radiation, seemingly small errors in the way the a_{CDOM} spectrum is measured or estimated can compound to become large errors in estimating biologically effective doses of UV to organisms using spectral UV models. This is because UV action spectra or biological weighting functions also often increase rapidly with decreasing UV wavelength. To illustrate this point, biologically effective doses of UV radiation were calculated using five a_{CDOM} spectra collected in the Dry Tortugas, Florida over a 24-hour period. For this example, UV attenuation by seawater and particulate matter was ignored, leaving CDOM absorption as the sole UV attenuator. A model noontime sea surface UV spectrum (Patterson, 1996) was multiplied by the Hunter *et al.* (1981) DNA biological weighting function (Figure 3a) and each of the five a_{CDOM} spectra (Figure 3b), resulting in five biologically weighted spectra (Figure 3c):

$$E(\lambda,z) = E(\lambda,0) \cdot \varepsilon(\lambda) \cdot a_{CDOM}(\lambda) \cdot z$$

$E(\lambda,z)$ = spectral irradiance at depth z (relative units)

$E(\lambda,0)$ = spectral irradiance at the sea surface ($\mu W\ cm^{-2}$)

$\varepsilon(\lambda)$ = biological response as a function of wavelength (relative

units)

$a_{CDOM}(\lambda)$ = spectral absorption by CDOM (m^{-1})

z = depth (1m in this example)

λ = wavelength (nm)

Finally, biologically effective UV doses (Figure 3d) were calculated by integrating the biologically weighted spectra in Figure 3c over all wavelengths. In this case, there was ~20% difference in the biologically effective dose due to CDOM absorption depending on which of the five a_{CDOM} sample spectra was chosen for the dose calculation. In this example, the differences in the a_{CDOM} spectra were most likely due to water column changes over the course of the 24-hour period. However, the

8

range of a_{CDOM} parameters presented is not wholly outside the range of values that might be observed if the same parcel of water were filtered and processed by multiple laboratories (personal experience). Great efforts were taken during the collection and processing of a_{CDOM} samples presented in this document to minimize sources of error due to loss of sample integrity and differences in sample processing methodologies and/or laboratory equipment.

In the following chapters, various aspects of UV attenuation and a_{CDOM} will be discussed. First, a description of the PRR/PUV and a_{CDOM} data collection methods will be discussed. Following the methods description, algorithms for estimating UV attenuation in surface waters from visible attenuation and remote sensing reflectances will be presented. In chapters 4 and 5, issues concerning the representation of the CDOM absorption spectrum and the importance of a_{CDOM} to total UV attenuation will be addressed. Subsequently, spatial and temporal patterns of UV attenuation and a_{CDOM} will be analyzed in the context of the other data collected and general environmental characteristics of each region. Lastly, there will be a summary and discussion of conclusions.

Some Existing Biological Weighting Functions
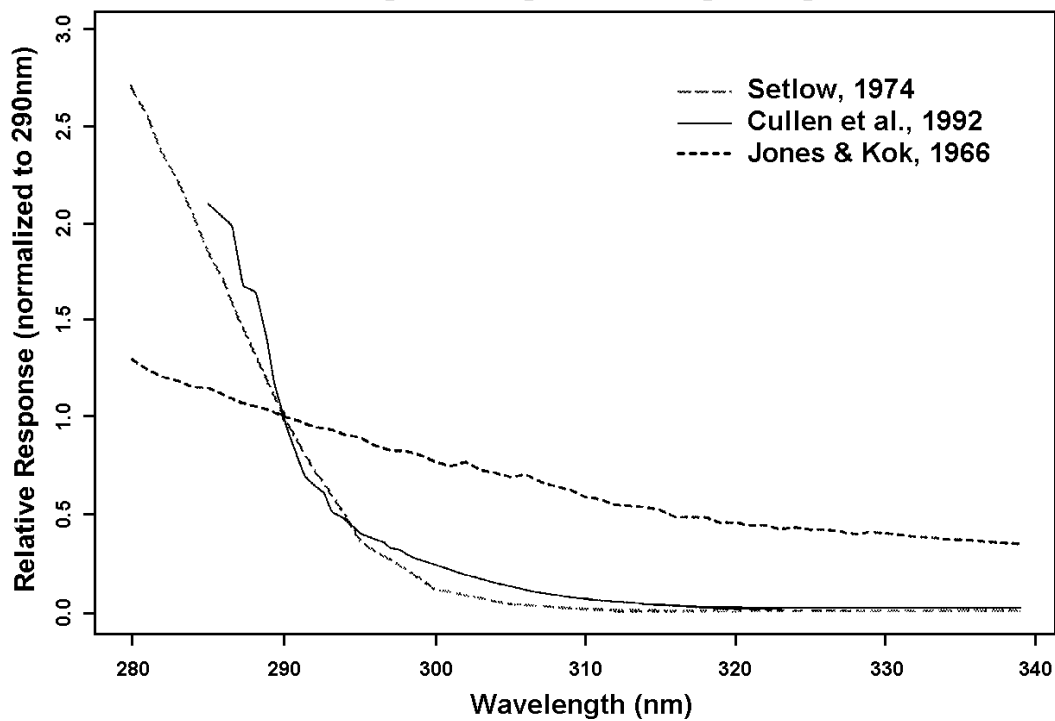
Figure 1: A sample of biological weighting functions existing in the literature showing the relative organism response as a function of wavelength. All curves have been normalized to 1 at 290nm. The curves plotted represent DNA damage (Setlow, 1974) and phytoplankton photoinhibition (Cullen *et al.*, 1992; Jones and Kok, 1966).

10

Example Spectra
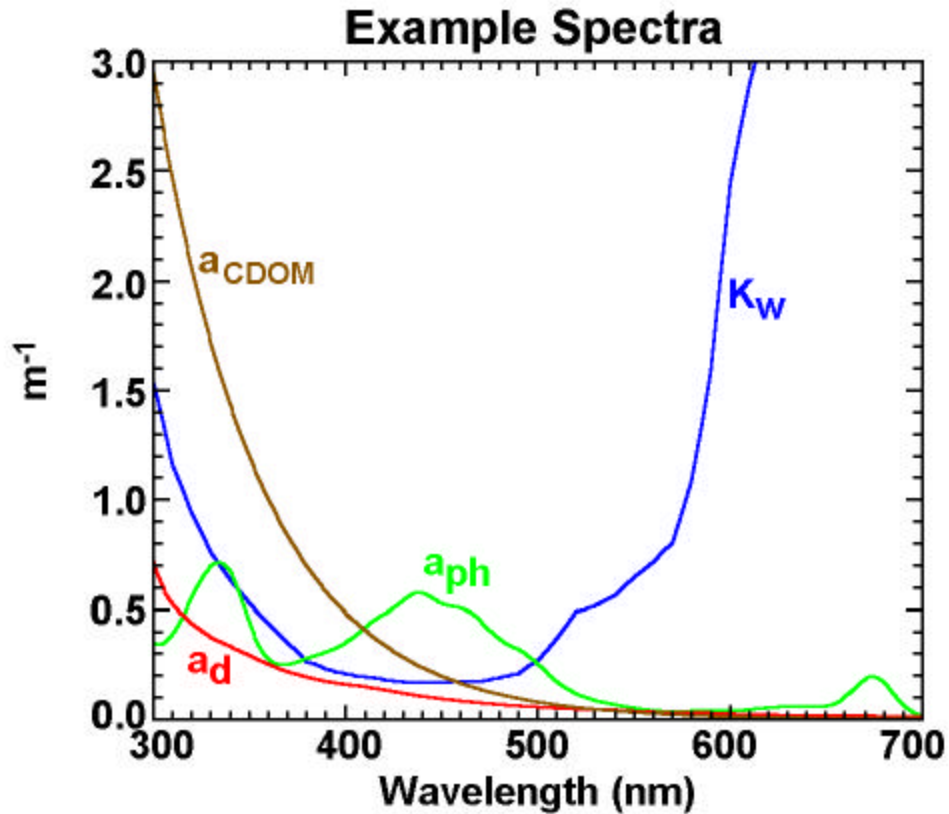
Figure 2: Some examples showing the shapes of the absorption or attenuation of UV and visible radiation by different components of seawater. K_w = the clearest natural water attenuation values of Smith and Baker (1981), which can be attributed mainly to pure seawater absorption in the visible, but includes some absorption by CDOM in the UV, a_{ph} = absorption by phytoplankton, a_d = absorption by non-living particulates (or detritus), a_{CDOM} = absorption by chromophoric dissolved organic matter. The Smith and Baker (1981) K_w values were plotted instead of pure water absorption (a_w) due to the lack of a reliable a_w spectrum in the 300-400nm range in the literature. The three absorption spectra plotted are for surface samples collected in the Antarctic on December 30, 1998.
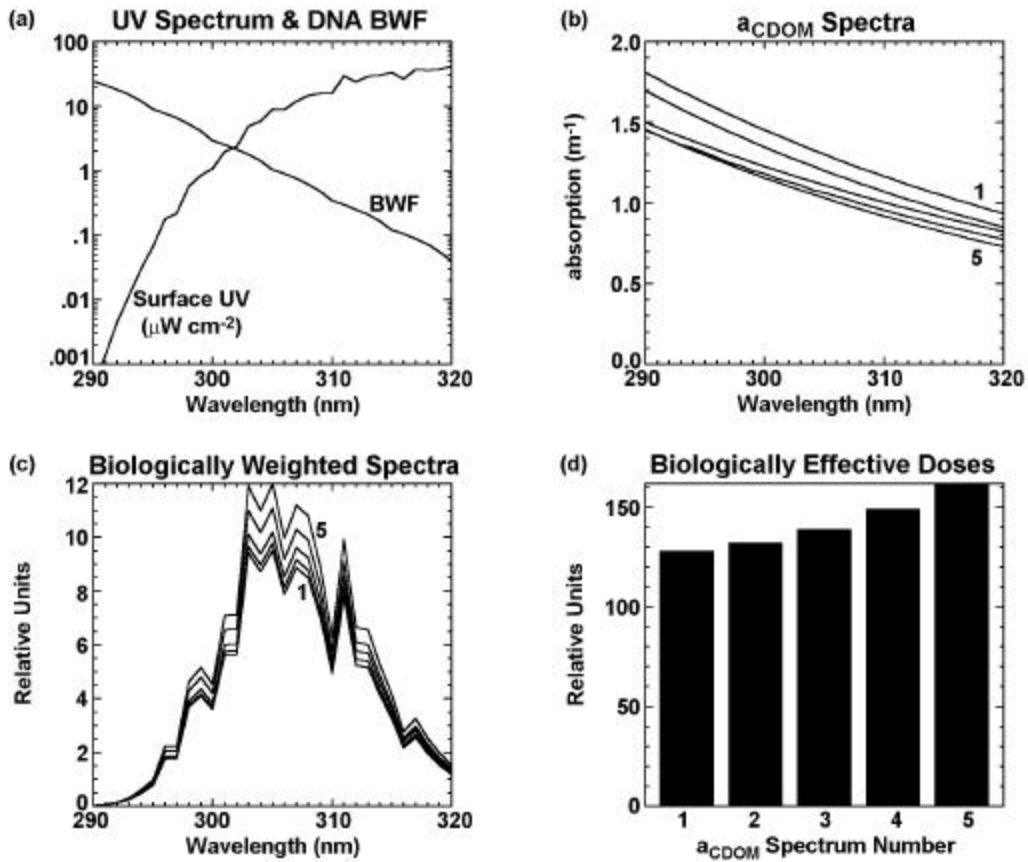
Figure 3: (a) An example model mid-latitude noontime surface UV spectrum for 300DU total column ozone (Patterson, 1996) plotted with the Hunter *et al.* (1981) DNA biological weighting function. (b) CDOM absorption spectra calculated using the following parameters from samples collected during the Dry Tortugas tidal cycle sampling in May 1998: spectrum 1: $a_{CDOM}(305) = 1.30m^{-1}$, $S = 0.022nm^{-1}$; spectrum 2: $a_{CDOM}(305) = 1.20m^{-1}$, $S = 0.023nm^{-1}$; spectrum 3: $a_{CDOM}(305) = 1.11m^{-1}$, $S = 0.020nm^{-1}$; spectrum 4: $a_{CDOM}(305) = 1.06m^{-1}$, $S = 0.021nm^{-1}$; spectrum 5: $a_{CDOM}(305) = 1.03m^{-1}$, $S = 0.023nm^{-1}$. Spectra are numbered 1-5 from top to bottom. (c) Biologically weighted spectra calculated by multiplying the surface UV spectrum in (a) by the biological weighting function in (a) and each of the a_{CDOM} spectra in (b). Curves 1-5 correspond to a_{CDOM} spectra 1-5 in (b) and are numbered from bottom to top. (d) Biologically effective UV dose calculated for each scenario by integrating over all wavelengths plotted in (c).

12

2. METHODS

2.1. General Data Collection

Data were collected in three contrasting coastal regions using a variety of platforms. These three regions, Santa Barbara Channel, Florida Keys and west Antarctic Peninsula, provide a wide range of optical water types, influenced by diverse processes. Sampling stations in each region are plotted in Figure 4 and a summary of data collected is given in Table 1.

2.1.1. Santa Barbara Channel

In the Santa Barbara Channel, data were collected as a part of the Plumes and Blooms project between September 1997 and July 1998. During this time period, there were several core cruises, which were day cruises sampling seven stations along a transect in the middle of the channel between Santa Rosa Island and the Goleta pier (Figure 4a). The National Oceanographic and Atmospheric Administration/Channel Islands National Marine Sanctuary (NOAA/CINMS) boat, R/V Ballena was used to collect samples on all core cruises. Wide ranges in type and amount of biogenous and terrigenous materials composed the waters sampled during this period.

There were also two multi-day process cruises during the study period. One of the process cruises was an eight-day cruise in October 1997 on board the NOAA ship, R/V MacArthur. During this cruise, samples were collected along a transect in the western Santa Barbara Channel, along a transect to the south of the Channel Islands towards San Nicholas Island, and in a region near the northern coast of Santa Rosa Island along with sampling the core transect twice during the cruise (Figure 4a). During

the cruise period, the waters were relatively clear and the sea and wind conditions were unusually calm over the eight-day period.

The second process cruise was conducted in February 1998 using the NOAA/CINMS R/V Ballena. Samples collected on this cruise were focused in the northeast region of the channel, but included the core transect as well (Figure 4a). The timing of the February 1998 cruise was planned to follow a large rain event in the local area to study the sediment plume produced by the Santa Clara and Ventura Rivers. This cruise followed quite a remarkable storm event. In the week prior to the three-day cruise, there were two large storms in the local area depositing a total of 10-28 inches of rain across Santa Barbara and Ventura counties. The second and larger storm occurred three days before the cruise and was accompanied by high winds, seas up to 26 feet high and wide spread flooding. On a SeaWiFS true-color composite image collected on February 9, 1998, brown sediment-laden water could be seen ten or more miles from the mainland coast with a green band of water extending from the edge of the brown water (Figure 5).

2.1.2. Florida Keys

Two two-week cruises were conducted in the Florida Keys region using the EPA ship, OSV Peter W. Anderson, as part of an EPA project studying coral diseases and the effects of multiple stressors on coral reefs. One cruise occurred during May/June 1998 and the other during September 1998. Water conditions were very unusual for this region during the May/June cruise. National Data Buoy Center climatological sea surface temperatures for the lower Florida Keys indicate water temperatures are generally in the range of 24-27°C during May (http://www.ndbc.noaa.gov/data/dataindex.shtml). The water was cooler

than normal, around 20°C in some places, and the water was visibly green with fast-growing macroalgae covering large reef areas. During the September cruise, water conditions were more typical, warmer and clearer with occasional tropical storm disturbances. Water column stratification also differed greatly between the two cruises. During the May/June cruise, there was often a distinct thermocline, with temperature differences between the surface and reef bottom up to 7-8°C. In contrast, the waters in September were more thermally mixed with temperature changes between the surface and reef bottom <0.5°C. Two types of platforms were used for data collection in this region. Water samples and optical casts were collected in shallow reef areas (Figure 4b) using either a small inflatable zodiac or one of the ship's RHIB's (Rigid Hulled Inflatable Boats). Deeper stations (Figure 4b) were sampled directly from the ship. In this region, the definition of a deep versus a shallow station is much different than in the other two regions studied. Bottom depths for reef stations were generally 1.5-8 meters and bottom depths for the CTD stations were generally 10-27 meters.

2.1.3. West Antarctic Peninsula

Two types of sampling regimes were employed in the west Antarctic Peninsula region. Two stations were sampled near Palmer Station off the south side of Anvers Island (Figure 4c inset) periodically from October 1998 through March 1999 using two Mark V zodiacs as part of the National Science Foundation Long Term Ecological Research Project (LTER). Unfortunately, due to ice and weather conditions, the zodiacs could only be launched for sampling about a dozen times during the four months dedicated to data collection from Palmer Station. A majority of the data collected in this region was collected during the LTER annual cruise in

January/February 1999. During the annual cruise, a rather large grid of stations (Figure 4c) was sampled over a period of five weeks using the ship, ARSV Laurence M. Gould. The zodiac stations near Palmer Station were also sampled three times during the cruise. Waters were generally ice-free and optically clear during the cruise. However, there were a few stations with optically dense waters, mainly in Marguerite Bay, located south of Adelaide Island (Figure 4c), where the one percent PAR (Photosynthetically Available Radiation, 400-700nm) level was found between 10-15m.

As the projects responsible for data collection in these three regions are large and interdisciplinary in scope, a rather large quantity and variety of data types are available for each region (Plumes and Blooms web site: http://www.icess.ucsb.edu/PnB/PnB.html, LTER web site: http://www.icess. ucsb.edu/lter/lter.html). Two types of optical datasets collected in all three regions using the same or very similar methods and instrumentation will be discussed here. One dataset consists of in-water optical profiles in the ultraviolet and visible portions of the solar spectrum at discrete wavelengths collected using a hybrid PRR/PUV instrument. The second dataset consists of spectral ultraviolet and visible absorption by chromophoric dissolved organic matter measured from discrete water samples using a spectrophotometer in the laboratory. Satellite imagery and other datasets, such as temperature, salinity, fluorometer and transmissometer data, collected in each region have been used when necessary to assist in interpreting results, however, the details of data collection methodology of those datasets will not be discussed.
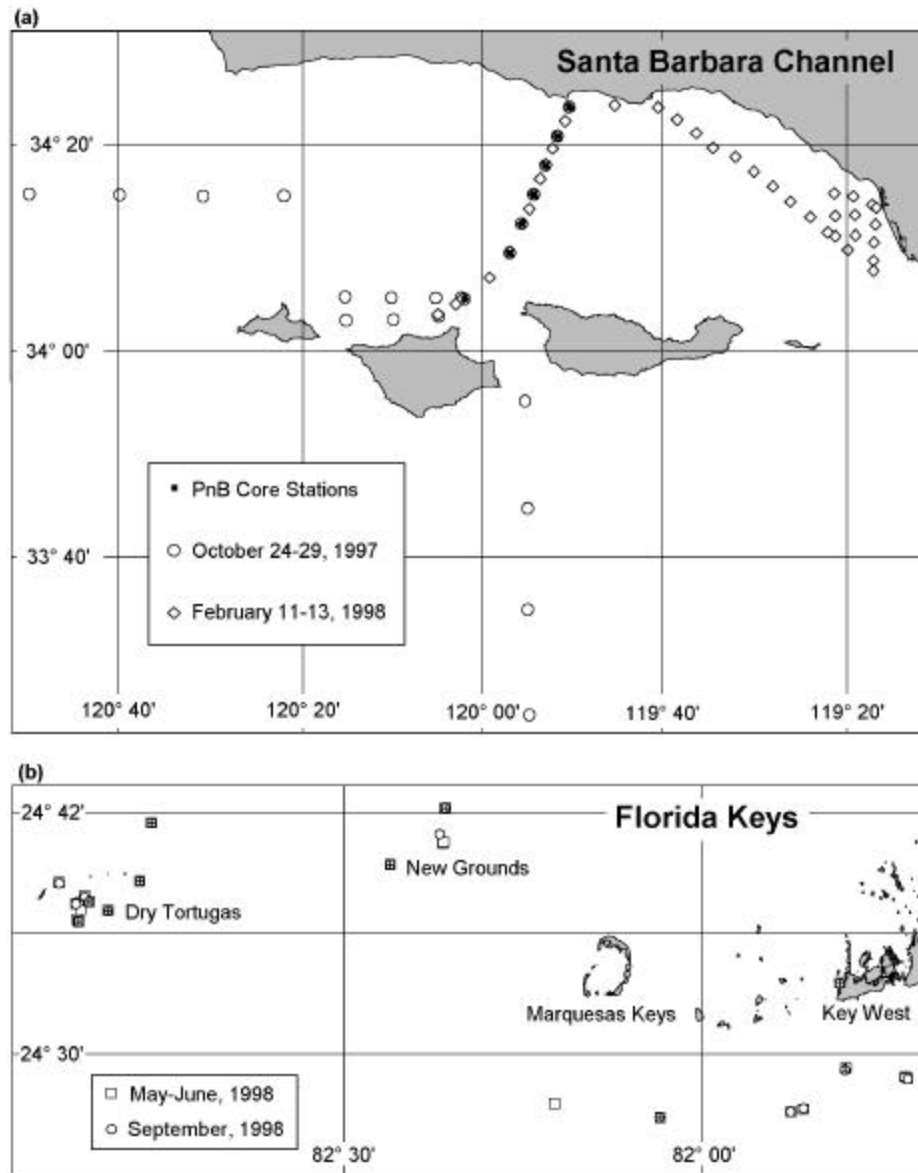
Figure 4: (a) Station locations for Plumes and Blooms cruises in the Santa Barbara Channel. Core cruises stations are numbered 1-7 from north to south. Water samples were collected at 0, 5, 10, 20, 30, 50 and 75m at station 4 and at the surface only at all other stations during core cruises. Water samples were collected at 0, 10, 20 and 30m at all stations during the October, 1997 cruise. In February, 1998, water samples were collected at 4 depths at 7 stations in the northeast corner of the channel and at the surface only at all remaining stations. (b) Station locations for EPA coral disease cruises in the Florida Keys. At each station, water samples were collected at the surface and 1m off the bottom. Symbols with a "+" in them represent deeper CTD stations. PRR/PUV casts were collected at all stations and all cruises plotted.

17
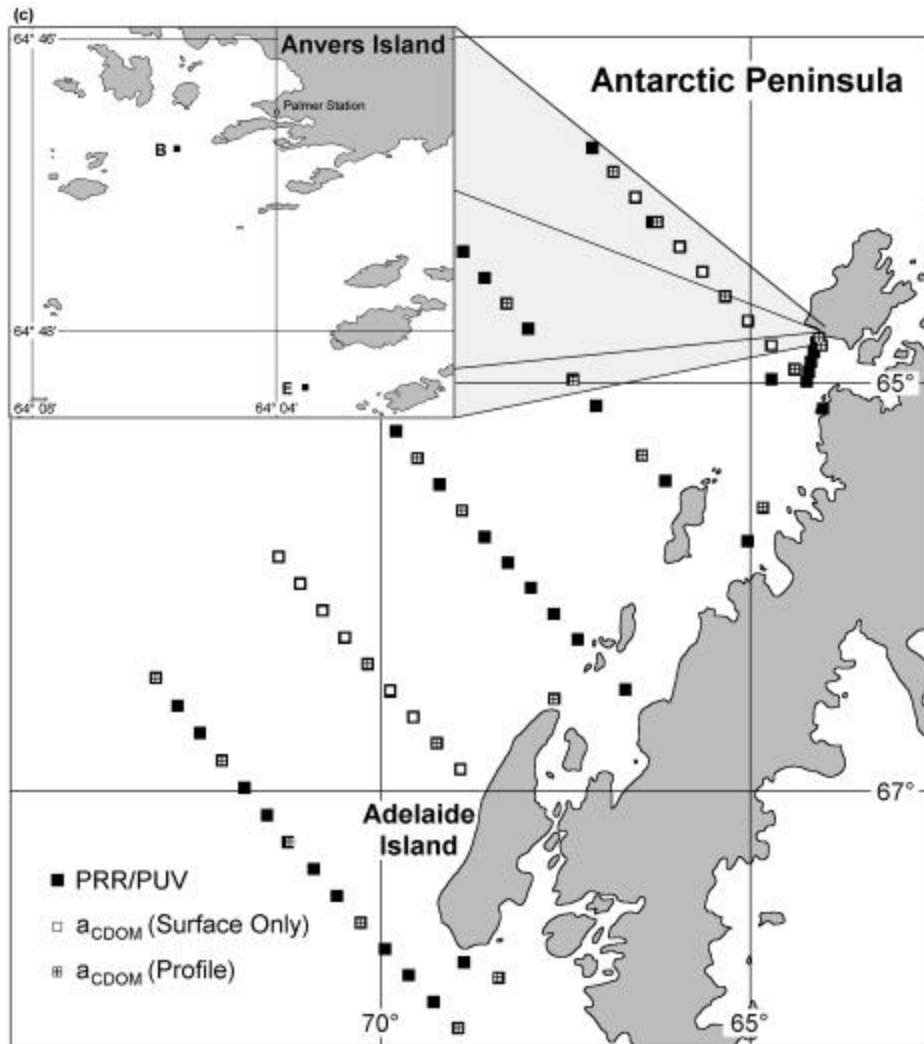
Figure 4: (c) LTER sampling stations in the west Antarctic Peninsula region. The large map shows stations sampled during the January/February 1999 cruise. PRR/PUV data are available for all stations plotted. Water samples for a_{CDOM} analysis were collected at 6 depths daily during the first half of the cruise and were collected from the station sampled closest to solar noon. These profile stations are depicted by a square with a "+" in it on the map. Two transect lines were repeated three weeks after initial sampling, collecting surface a_{CDOM} samples only at all stations along these repeat transects. Sampling sites along the repeat transects are depicted as open boxes. The inset shows the two stations (B and E) sampled via zodiac in the Palmer Station local area. Periodic PRR/PUV casts and profile a_{CDOM} water samples were collected at stations B and E from October, 1998 – March, 1999. Water sampling depths for both zodiac and shipboard collections were chosen based on percent light level and samples were collected at the 100, 60, 30, 10, 5 and 1% PAR depths.
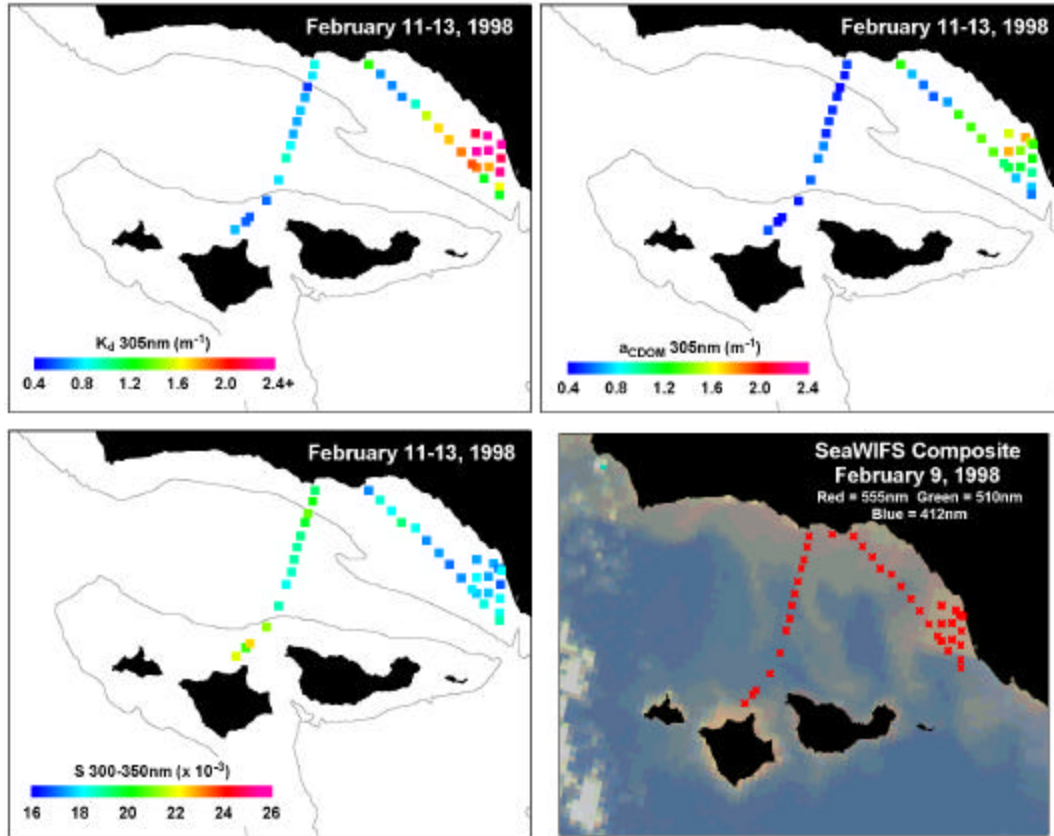
Figure 5: Ultraviolet attenuation at 305nm for the upper 10m of the water column, $a_{CDOM}(305)$ and S(300-350) for the February, 1998 sediment plume process cruise in the Santa Barbara Channel. Spatial patterns observed matched closely to sediment plume patterns observed on the SeaWiFS "true color" visible composite image. The 200m bathymetry contour is plotted for reference.

Table 1: Summary of PRR/PUV casts and a_{CDOM} samples collected in each region. The number of total a_{CDOM} samples collected from the top 1m of the water column are given in parentheses.

Dataset	Total # PRR/PUV Casts	Total # a_{CDOM} samples (surface only)	Start Date	End Date
Santa Barbara Channel Core Cruises	64	94 (53)	9/19/97	7/13/98
Santa Barbara Channel October 1997	29	128 (34)	10/24/97	10/29/97
Santa Barbara Channel February 1998	38	59 (38)	2/11/98	2/13/98
Florida Keys May 1998	22	64 (32)	5/23/98	6/2/98
Florida Keys September 1998	18	55 (27)	9/3/98	9/11/98
Antarctic Peninsula Palmer 9899	24	108 (20)	10/21/98	3/2/99
Antarctic Peninsula January 1999	88	166 (42)	1/8/99	2/11/99
Total	283	674 (246)	9/19/97	3/2/99

2.2. PRR/PUV

The PRR/PUV instrument is a hybrid instrument constructed by Dave Menzies at the University of California – Santa Barbara from two independent instruments, the PRR (Profiling Reflectance Radiometer) and the PUV (Profiling Ultraviolet Radiometer), both manufactured by Biospherical Instruments, Inc. The instrument has five optical sensor heads – surface downwelling UV irradiance, surface downwelling visible irradiance, in-water downwelling UV irradiance, in-water downwelling visible irradiance and upwelling visible radiance. Downwelling irradiance is measured at 305, 320, 340, 380, 412, 443, 490, 510, 555, 656nm and broadband PAR (400-700nm) and upwelling radiance is measured at 412, 443, 490, 510, 555, 656 and 683nm. Most of these channels have a bandwidth of ~8-10nm. The two exceptions are the 305nm channel, which has an effective bandwidth of ~15nm, and the broadband PAR channel. The profiling unit of the PRR/PUV is encased in Delrin. The two Delrin cans are connected with a short data cable for simultaneous integrated measurements of UV and visible data and are outfitted with a common floatation collar and fins to allow maintenance of vertical orientation in the water column during free-fall deployment (Waters *et al.*, 1990).

Though many different platforms were used to collect the PRR/PUV data, the method of deployment was the same. The deck units were mounted in a location easily accessible for cleaning, but minimally shaded by higher parts of the vessel and passersby. The profiling unit was floated away from the vessel about 20m on the sunny side, when possible. Then the computer data collection software was started and the instrument was allowed to free-fall through the water column. The descent rate of the profiling unit was adjusted with lead sinkers for optimal data collection. In

the Santa Barbara Channel and in the Antarctic, the descent rate was about 0.5m/s, giving approximately 2-3 scans per meter. In the shallow waters of the Florida Keys, where station depths were often <7m, a descent rate of 0.5m/s was too fast, resulting in only a few quality scans per cast. Therefore, the descent rate was slowed to about 0.2m/s in the Florida Keys, giving approximately 6-8 scans per meter. This slower descent rate ensured there was at least 10-15 good quality scans collected at even the shallowest station. Dark values were collected by placing dark caps over all sensor windows at the conclusion of each cast.

Casts were processed by first extracting only downcast data. From the downcast data, scans collected with high instrument tilt and/or roll values were eliminated and each cast was plotted for visual inspection to eliminate any suspect portions, such as those resulting from ship shadow or a small, but dense cloud moving quickly past the solar disk. For each cruise, instrument calibration was checked and adjusted if needed. All dark scans collected during each cruise were combined and a linear temperature-dependent dark voltage correction value was calculated for each of the deck unit channels. For the profiling unit, an average dark value was calculated for each channel and initially applied to each cast. Then, each cast was plotted one channel at a time on a log-linear scale and the dark value was adjusted, if needed as recommended in the PUV manual (1992), so the datapoints fanned out as they approached the detection limit of the channel rather than curving to one side or the other.

Two types of derived data products were calculated from processed downcasts. First, an average diffuse attenuation coefficient ($K_{Ed}(\lambda)$ for downwelling irradiance or $K_{Lu}(\lambda)$ for upwelling radiance) was calculated for all scans collected between just below the sea surface and 10m of each cast (hereafter referred to as "top 10m" values). Scans collected deeper

than 10m were eliminated from calculations for this study for two reasons. First, the depth range chosen needed to be deep enough to minimize the effects of data scatter due to wave action and small fluctuations in instrument orientation at the beginning of a cast. Second, the depth needed to be shallow enough to be above the detection limit of most or all of the channels under a majority of water compositions encountered. The UV channel which approaches the detection limit first is the 305nm channel, reaching the detection limit by 10-15m depth in most cases. In the event that the detection limit or the bottom was reached before 10m, all valid data scans for the cast were used. Attenuation coefficients were calculated using Beer's Law:

$$E(\lambda, z_2) = E(\lambda, z_1) \cdot e^{-K(\lambda)[z_2 - z_1]}$$

$E(\lambda, z_2)$ = irradiance at wavelength λ, depth z_2

$E(\lambda, z_1)$ = irradiance at wavelength λ, depth z_1

$K(\lambda)$ = diffuse attenuation coefficient at wavelength λ (m^{-1})

z_1, z_2 = two different depths (m)

Irradiance or radiance values for each channel were plotted versus depth on a log-linear scale and a least-squares line was fit to all datapoints collected between the surface and 10m. Rewriting Beer's Law to resemble the general equation of a line, it follows that the slope of the least-squares fit line is the attenuation coefficient.

$$\ln(E(\lambda, z_2)) = K(\lambda)[z_1 - z_2] + \ln(E(\lambda, z_1))$$

The second type of derived product that was calculated was the surface irradiance or radiance value. The irradiance or radiance value just below the sea surface ($E_d(\lambda, 0^-)$ or $L_u(\lambda, 0^-)$) was calculated using a similar method to the attenuation coefficient calculations. All valid datapoints from the top 10m of each cast were plotted versus depth on a log-linear scale and an

irradiance (radiance) value was calculated from a least-squares line fit at a depth of zero meters.

2.3. a_{CDOM}

Spectrophotometric ultraviolet and visible light absorption by chromophoric dissolved organic matter (a_{CDOM}) was measured from water samples collected in each region using 10cm pathlength quartz cuvettes. Before continuing, it is important to operationally define a_{CDOM}. Using the laboratory process described in this section, a_{CDOM} is defined as all seawater components smaller than 0.2μm in size (other than water molecules), which absorb radiation in the 250-700nm range.

General sample collection and processing techniques were similar for all datasets. Prior to sample collection, amber glass bottles with teflon insert lids were thoroughly acid washed and rinsed with organic-free water. Bottles were then stored in the refrigerator full of organic-free water until ready for use. Throughout sample collection and processing, sample bottles were kept in the dark at all times to avoid photodegradation. All sample bottles were rinsed three times with sample water prior to filling them with sample water. Polycarbonate membrane filters with a 0.2μm pore size were placed on a clean all-glass filtration tower and were pre-washed with 80-100ml organic- free water, followed by three or four rinses with 10-15ml sample water. The filter flask was shaken and emptied after each rinse to ensure the filter flask was properly seasoned for the current sample. The remaining sample was then filtered at a vacuum pressure of no more than 12 inHg. At no time was sample water allowed to run dry on the filter. After filtering, the amber glass sample bottle was rinsed thoroughly with organic-free water, then rinsed three times with the filtered sample water and refilled with the filtered sample water. Samples were

then brought to room temperature for spectrophotometric analysis using 10-cm pathlength quartz cuvettes cleaned with HPLC grade ethanol prior to each scan. All seawater samples and reference blanks consisting of organic-free water were scanned from 250-750nm at 0.5nm intervals, using a slit width of 4nm with a 2nm smoothing. Samples were scanned multiple times (usually 3 times), cleaning and refilling the cuvette between each scan. The precision level of the instruments used was 0.001-0.002OD, which translates to an absorption coefficient precision of 0.023-0.046m^{-1}.

While general sample collection and processing were similar, there were some modifications made for each region due to logistical constraints. In the Santa Barbara Channel region, Niskin bottles mounted on the CTD rosette were used to collect all water samples. Unfiltered samples were refrigerated for several hours prior to filtering. All samples were filtered the evening of collection within 12 hours of collection. When possible, filtered samples were scanned immediately after filtering. When it was not possible to immediately scan filtered samples, samples were stored in the refrigerator at 4°C until ready to scan. All core cruise samples were scanned within 24 hours of collection. Process cruise samples collected in October 1997 and February 1998 were all scanned within one week of collection. A set of samples was checked in July 1997 for preservation after storage in a refrigerator for a three-week period. Spectra measured after the three-week storage period were within the measurement error of the spectrophotometer. Reference water used in this region was water drawn from a Millipore Alpha-Q water system and a Perkin-Elmer Lambda 2 spectrophotometer was used to scan samples.

In the Florida Keys region, there were three methods of sample collection. Surface water samples at reef stations were collected by submerging the amber glass sample bottle just below the sea surface.

Samples collected just off the reef bottom were collected using a van Dorn bottle. Samples collected at the somewhat deeper CTD stations were collected using Go-Flo bottles pre-rinsed with alcohol and mounted on the CTD rosette. Unfiltered samples were kept cold either in the refrigerator or in a cooler on ice for up to 6 hours before filtering. After each cruise, samples were packaged in coolers with blue ice and shipped overnight to Santa Barbara for scanning using the same Perkin-Elmer Lambda 2 spectrophotometer used for scanning Santa Barbara Channel samples. All samples were scanned within 2 weeks of collection. Due to logistical constraints, it was not possible to test samples to verify preservation over the two-week period, however, sample handling methods were comparable to those used for Santa Barbara Channel samples, which preserved well for three weeks in laboratory testing. The reference water used in this region was Alpha-Q water from the same system used to process the Santa Barbara Channel samples.

In the Antarctic, all samples were collected using Go-Flo bottles. Samples in this region needed to be kept between -2°C and 0°C to avoid significant degradation prior to filtration. This was accomplished by either keeping the samples in a cooler outside when the air temperature was at or below freezing or in a cooler filled with ice or snow. All samples were filtered within 24 hours of collection and a vast majority were scanned immediately after filtering. Three sources of reference water were used for this region. At Palmer Station, reference water was drawn from either a Barnstead-Thermolyne OrganicPure system or a Barnstead-Thermolyne E-Pure system. On the LTER January 1999 cruise, reference water was obtained from a Millipore $H_2O\infty$ system. There were two Perkin-Elmer Lambda 6 spectrophotometers used at various times to scan samples in

this region due to the development of several instrument maintenance problems through the season.

Post-processing of spectral scans consisted first of adjusting for instrument drift and features. Since a_{CDOM} values drop off exponentially with increasing wavelength in the visible, seawater absorption is well within the detection limit of the instrument by 700nm. Therefore, each scan was adjusted to a value of zero at 700nm. To account for any non-sample spectral variations, reference spectra of organic-free water were scanned approximately every fourth scan and the appropriate reference spectrum was subtracted from each sample scan. Next, replicate scans for each sample were plotted together and any outliers or suspect scans were deleted. Remaining scans were averaged and instrument optical densities were converted to seawater absorption coefficients in units of m^{-1} by multiplying by 2.303 to convert from $\log_{10}$ to natural log units and dividing by the pathlength of the cuvette, which was 0.10m.

3. ESTIMATING UV ATTENUATION FROM VISIBLE MEASUREMENTS

Measurements of UV radiation in the coastal and open ocean are widely scattered over the globe in space and time. Comparisons of available UV datasets are often difficult due to large variations in spectral ranges and resolutions of instruments used currently and in the past. Comparisons between instruments are often complicated further due to differences in the way instruments are designed to measure UV radiation in the water column, whether it be a difference of bandwidth, a difference of counting photons versus measuring total energy, a difference in making instantaneous versus time-integrated measurements, a difference in sensor window design, a difference in signal-to-noise ratio or a difference between a profiling instrument and a static-depth instrument.

However, while UV measurements are widely scattered and varied, the visible ocean optics community has, in comparison, rather large reservoirs of more standardized datasets available spawned from the development of airplane, CZCS (Coastal Zone Color Scanner), SeaWiFS and other ocean color satellite sensors. These visible datasets could prove useful in estimating UV attenuation in coastal seawater where UV measurements would otherwise be unavailable provided relationships are established between UV attenuation and measurements of attenuation and/or reflectance made at visible SeaWiFS wavelengths. Collection of over 200 casts in waters of vastly different water masses with the PRR/PUV instrument provided a situation whereby such statistical relationships between UV attenuation and SeaWiFS wavelengths could be made. A wide variety of water compositions were sampled so that the global applicability of algorithms could be assessed.

29

Average attenuation coefficients and irradiance/radiance values just below the sea surface calculated from the top 10 meters of each PRR/PUV cast were used for this analysis. For SeaWiFS wavelengths, remote sensing reflectances were calculated as $R_{rs}(\lambda) = C_1 \cdot L_u(\lambda,0^-)/[C_2 \cdot E_d(\lambda,0^-)]$, where λ is wavelength, $L_u(\lambda,0^-)$ is upwelling radiance just below the sea surface, $E_d(\lambda,0^-)$ is downwelling irradiance just below the sea surface, and C_1 and C_2 are spectral invariant constants to account for radiance reflection at and transmission through the air-water interface. On average, $C_1 = 0.54$ and $C_2 = 1.04$, however, these values vary somewhat with sea state (Austin, 1974). For simplification, the constants, C_1 and C_2, have been excluded in calculations. Correlation coefficients were calculated for $K_{E_d}(305)$, $K_{E_d}(320)$, $K_{E_d}(340)$ and $K_{E_d}(380)$ plotted versus K_{E_d} and K_{L_u} for each of the visible channels. Correlation coefficients were also calculated for $K_{E_d}(UV)$ values plotted versus remote sensing reflectances at SeaWiFS wavelengths and all combinations of remote sensing reflectance wavelength pair ratios.

For better understanding, each region was analyzed separately before combining datasets for determining more globally applicable relationships. All Santa Barbara Channel cruises, excluding high sediment load plume waters encountered during the February 1998 process cruise, were analyzed as a single dataset. High sediment plume waters were defined as profiles where $K_{E_d}(305)$ was greater than $2m^{-1}$. Ultraviolet attenuation coefficients greater than this value were calculated using only a few data scans collected within a very shallow surface layer and were highly unreliable. Attenuation coefficients for profiles collected outside the main plume during the February 1998 cruise were within the variability encountered in the Santa Barbara Channel during regular core cruises and

were retained for analysis. In the Florida Keys region, the May 1998 and September 1998 cruises were analyzed separately due to the unusual water conditions encountered in May 1998. Due to instrument limitations in very shallow waters, including instrument self-shading and bottom reflections dominating the upwelling radiance signal, K_{L_u} and remote sensing reflectances could not be calculated for the Florida Keys region. In the west Antarctic Peninsula region, the relatively few profiles collected during the Palmer Station zodiac season were combined with profiles collected during the January 1999 cruise and were considered as a single dataset.

No *a priori* assumptions were made as to which visible wavelengths or wavelength ratios would be most useful for such correlation analysis to avoid introducing biases into the analyses. However, since CDOM and detrital material absorb more strongly with decreasing wavelength and phytoplankton also absorb strongly in the blue region of the spectrum (Figure 2), one would expect measurements at 412 or 443nm to provide the best chance of estimating UV absorbing components in the water column. Existing ocean color algorithms have found 443 and 490nm wavelength channels to be most useful in algorithm development for the estimation of chlorophyll due to the strong chlorophyll absorption band in this region (O'Reilly *et al.*, 1998). The 412nm wavelength channel proved much less useful in chlorophyll algorithm development due to increased CDOM and detrital absorption at this shorter wavelength (O'Reilly *et al.*, 1998). Therefore, the 412nm channel would be expected to include the best balance of UV absorbing components of seawater for developing UV attenuation algorithms.

When developing remote sensing reflectance algorithms, wavelength pair ratios have the advantage over single wavelength

algorithms due to a decreased sensistivity to sea state. The spectrally invariant constants accounting for transmission through the air-water interface, C_1 and C_2, cancel out in the wavelength pair ratio calculation, making the wavelength pair ratio less sensitive to changes in C_1 and C_2 with sea state (Austin, 1974). Of the SeaWiFS channels, the 555nm channel is expected to be the best companion wavelength for developing remote sensing reflectance wavelength pair algorithms, since both particulate and dissolved organic matter absorb weakly in this spectral region (Figure 2). Indeed, the 555nm channel has proved useful in remote sensing reflectance wavelength pair algorithms for estimating chlorophyll from ocean color (O'Reilly *et al.*, 1998).

With the exception of the Florida Keys – May 1998 cruise, UV attenuation coefficients highly correlated with $K_{E_d}(412)$, $K_{L_u}(412)$ and the ratio of $R_{rs}(555)/R_{rs}(412)$ in all regions (Figures 6-8, Table 2). Visual analysis of plots of UV attenuation coefficients versus $K_{E_d}(412)$ (Figure 6) indicates higher relative UV attenuation in the Florida Keys – May 1998 dataset compared to the other three datasets. On these plots, increased elevation of the Florida Keys – May 1998 UV attenuation coefficients with decreasing wavelength can be seen. Both CDOM and detrital particles have spectral signatures which progressively increase with decreasing wavelength across the UV-VIS spectrum, indicating the Florida Keys – May 1998 waters had higher CDOM and/or detrital influence compared to attenuation by phytoplankton. Indeed, further analysis of a_{CDOM} samples versus UV attenuation coefficients indicates domination of UV attenuation coefficients in the Florida Keys – May 1998 cruise by a_{CDOM} (Figure 9).

Comparing the slopes of least-squares linear fits for each dataset (Figures 6-7, Table 2), the Antarctic Peninsula region exhibits significantly

32

lower slopes than the other study regions for K(UV) versus $K_{E_d}(412)$ and $K_{L_u}(412)$. In contrast to the Florida Keys – May 1998 dataset, the spectral pattern for the Antarctic Peninsula compared to the other datasets suggests very low contribution by a_{CDOM} compared to absorption by phytoplankton.   Again, this conclusion has been confirmed with comparisons of spectrophotometric a_{CDOM} measurements and K(UV) (Figure 9). In fact, a_{CDOM} was often below the detection range of the spectrophotometer at wavelengths longer than 320-350nm in the Antarctic, while detection often remained into the visible range in the other two regions.   Interestingly, relationships between K(UV) and $R_{rs}(555)/R_{rs}(412)$ (Figure 8, Table 2) were remarkably similar for both the Antarctic Peninsula and Santa Barbara Channel regions, indicating $R_{rs}(555)/R_{rs}(412)$ is a remote sensing reflectance ratio with great utility across waters of highly differing composition.   The utility of the $R_{rs}(555)/R_{rs}(412)$ ratio was not expected as Mitchell and Holm-Hansen (1991) have found that regional remote sensing wavelength pair algorithms were necessary to accurately estimate chlorophyll concentrations in the Antarctic Peninsula region due to pigment-packaging effects and low CDOM and detrital concentrations compared to other regions of the globe.

Table 2: Linear fit parameters (slope and intercept) and correlation coefficients (r^2) for lines plotted in Figures 6-8. Ultraviolet attenuation can be estimated using $K_{E_d}(\lambda)$ = Channel(Slope) + Intercept, where Channel, Slope and Intercept are the column headings listed below. The number of casts used from each region is: Florida Keys – May98 (22 casts); Florida Keys – Sep98 (16 casts); Santa Barbara Channel (116 casts); Antarctic Peninsula (112 casts).

$K_{E_d}(305)$

Dataset	Channel	Slope	Intercept	r^2
Florida Keys - May98	$K_{E_d}(412)$	3.378	0.429	0.51
Florida Keys - Sep98	$K_{E_d}(412)$	2.020	0.325	0.91
Santa Barbara Channel	$K_{E_d}(412)$	1.637	0.249	0.76
Antarctic Peninsula	$K_{E_d}(412)$	1.460	0.178	0.75
All (no FK May98)	$K_{E_d}(412)$	1.971	0.180	0.77
Santa Barbara Channel	$K_{L_u}(412)$	1.746	0.200	0.68
Antarctic Peninsula	$K_{L_u}(412)$	1.180	0.188	0.85
Santa Barbara + Antarctic	$K_{L_u}(412)$	1.754	0.165	0.72
Santa Barbara Channel	$R_{rs}(555)/R_{rs}(412)$	0.341	0.207	0.88
Antarctic Peninsula	$R_{rs}(555)/R_{rs}(412)$	0.356	0.162	0.81
Santa Barbara + Antarctic	$R_{rs}(555)/R_{rs}(412)$	0.360	0.176	0.89

$K_{E_d}(320)$

Dataset	Channel	Slope	Intercept	r^2
Florida Keys - May98	$K_{E_d}(412)$	2.951	0.222	0.70
Florida Keys - Sep98	$K_{E_d}(412)$	1.871	0.192	0.94
Santa Barbara Channel	$K_{E_d}(412)$	1.484	0.167	0.86
Antarctic Peninsula	$K_{E_d}(412)$	1.201	0.117	0.87
All (no FK May98)	$K_{E_d}(412)$	1.750	0.106	0.83
Santa Barbara Channel	$K_{L_u}(412)$	1.602	0.119	0.77
Antarctic Peninsula	$K_{L_u}(412)$	0.948	0.127	0.92
Santa Barbara + Antarctic	$K_{L_u}(412)$	1.576	0.092	0.78
Santa Barbara Channel	$R_{rs}(555)/R_{rs}(412)$	0.303	0.135	0.91
Antarctic Peninsula	$R_{rs}(555)/R_{rs}(412)$	0.357	0.077	0.87
Santa Barbara + Antarctic	$R_{rs}(555)/R_{rs}(412)$	0.327	0.103	0.92

Table 2: (continued)

$K_{E_d}(340)$

Dataset	Channel	Slope	Intercept	r^2
Florida Keys - May98	$K_{E_d}(412)$	2.220	0.124	0.80
Florida Keys - Sep98	$K_{E_d}(412)$	1.563	0.106	0.95
Santa Barbara Channel	$K_{E_d}(412)$	1.317	0.101	0.90
Antarctic Peninsula	$K_{E_d}(412)$	1.096	0.066	0.90
All (no FK May98)	$K_{E_d}(412)$	1.485	0.058	0.88
Santa Barbara Channel	$K_{L_u}(412)$	1.389	0.062	0.84
Antarctic Peninsula	$K_{L_u}(412)$	0.879	0.075	0.94
Santa Barbara + Antarctic	$K_{L_u}(412)$	1.358	0.046	0.84
Santa Barbara Channel	$R_{rs}(555)/R_{rs}(412)$	0.263	0.077	0.92
Antarctic Peninsula	$R_{rs}(555)/R_{rs}(412)$	0.340	0.024	0.88
Santa Barbara + Antarctic	$R_{rs}(555)/R_{rs}(412)$	0.283	0.055	0.92

$K_{E_d}(380)$

| Dataset	Channel	Slope	Intercept	r^2
Florida Keys - May98	$K_{E_d}(412)$	1.462	0.014	0.93
Florida Keys - Sep98	$K_{E_d}(412)$	1.192	0.021	0.98
Santa Barbara Channel	$K_{E_d}(412)$	1.091	0.024	0.96
Antarctic Peninsula	$K_{E_d}(412)$	0.912	0.021	0.97
All (no FK May98)	$K_{E_d}(412)$	1.135	0.010	0.95
Santa Barbara Channel	$K_{L_u}(412)$	1.109	-0.003	0.90
Antarctic Peninsula	$K_{L_u}(412)$	0.759	0.025	0.95
Santa Barbara + Antarctic	$K_{L_u}(412)$	1.050	0.001	0.90
Santa Barbara Channel	$R_{rs}(555)/R_{rs}(412)$	0.211	0.010	0.92
Antarctic Peninsula	$R_{rs}(555)/R_{rs}(412)$	0.285	-0.015	0.92
Santa Barbara + Antarctic	$R_{rs}(555)/R_{rs}(412)$	0.218	0.010	0.92
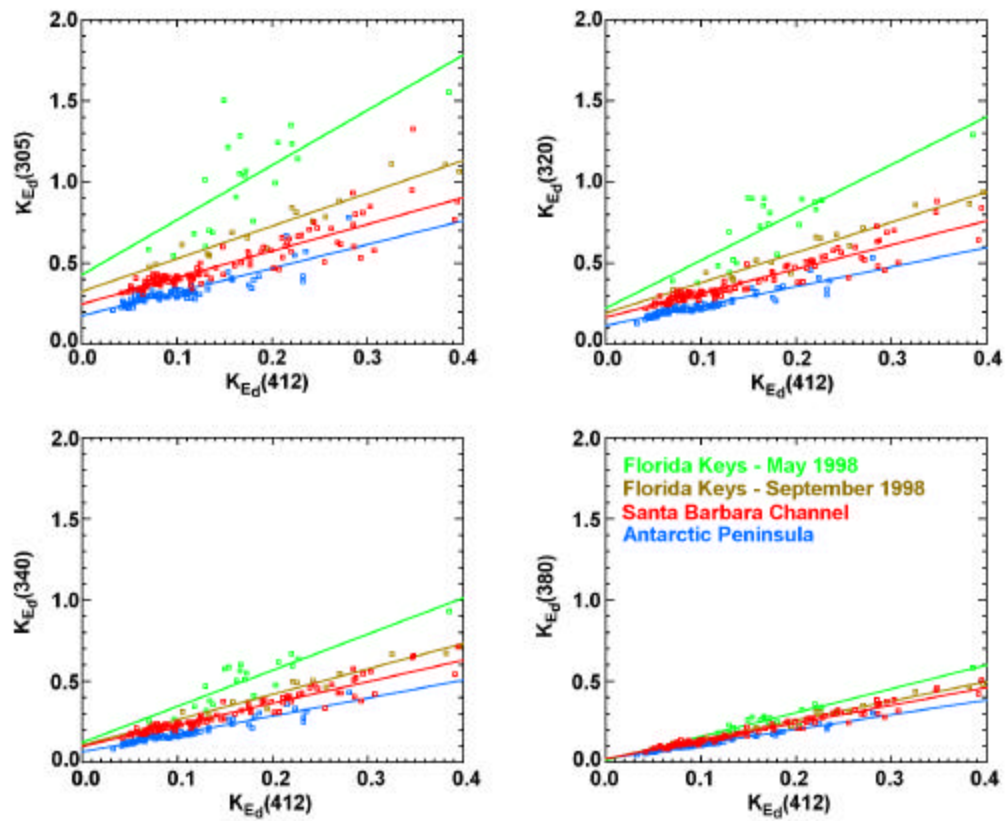
Figure 6: $K_{E_d}(UV)$ plotted versus $K_{E_d}(412)$ with least-squared linear fits for each study region. Attenuation coefficients were calculated from data collected in the top 10m of each profile. All casts with $K_{E_d}(305) > 2m^{-1}$ were excluded from this analysis due to high potential calculation errors arising from lack of datapoints in the cast.
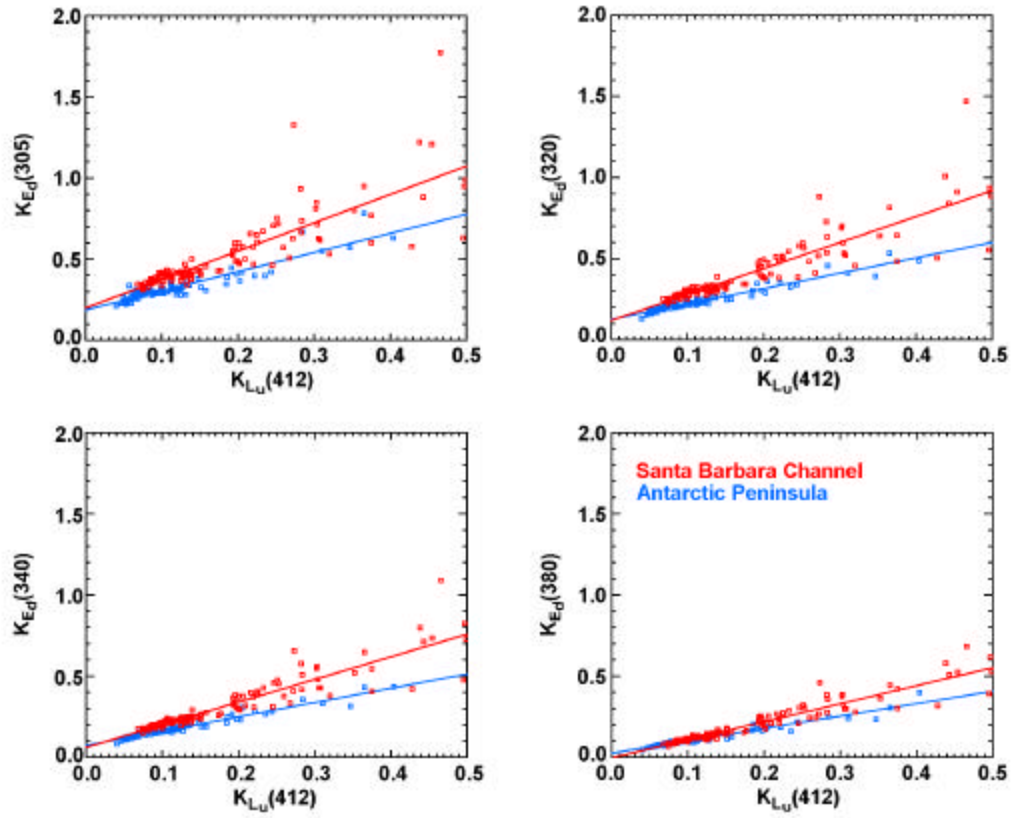
Figure 7: Same as Figure 6 for $K_{E_d}(UV)$ versus $K_{L_u}(412)$ in the Santa Barbara Channel and Antarctic Peninsula regions.
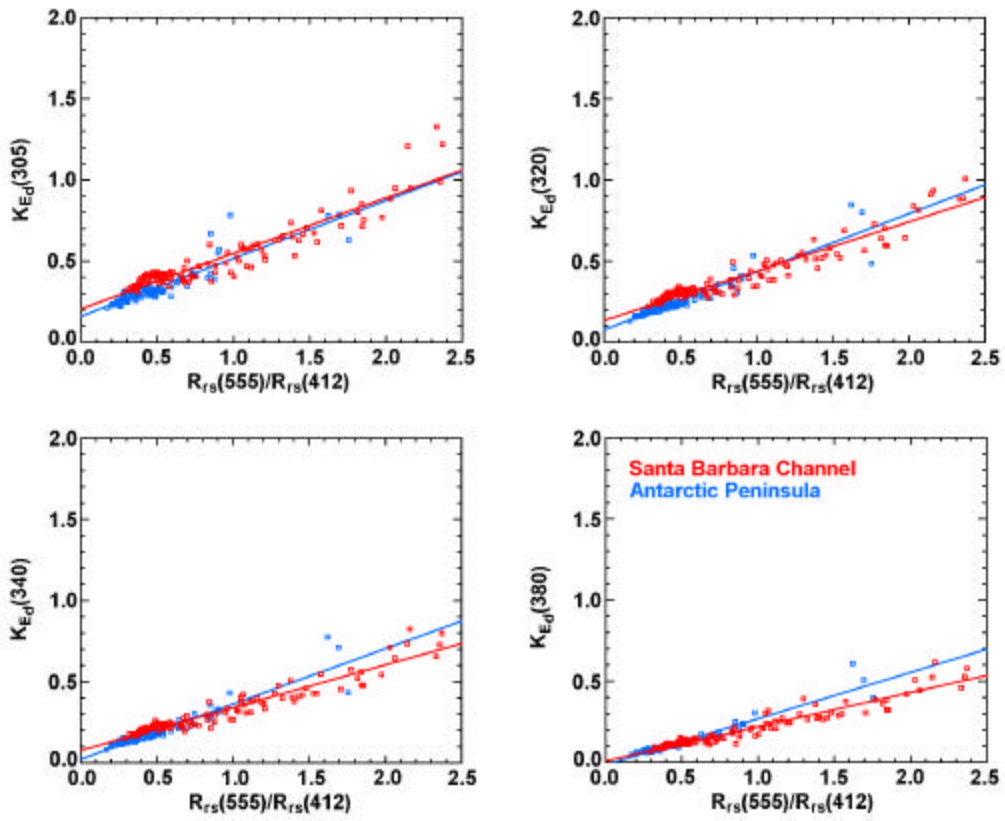
Figure 8: Same as Figure 6 for $K_{E_d}(UV)$ versus the remote sensing reflectance ratio $R_{rs}(555)/R_{rs}(412)$ for the Santa Barbara Channel and Antarctic Peninsula regions.
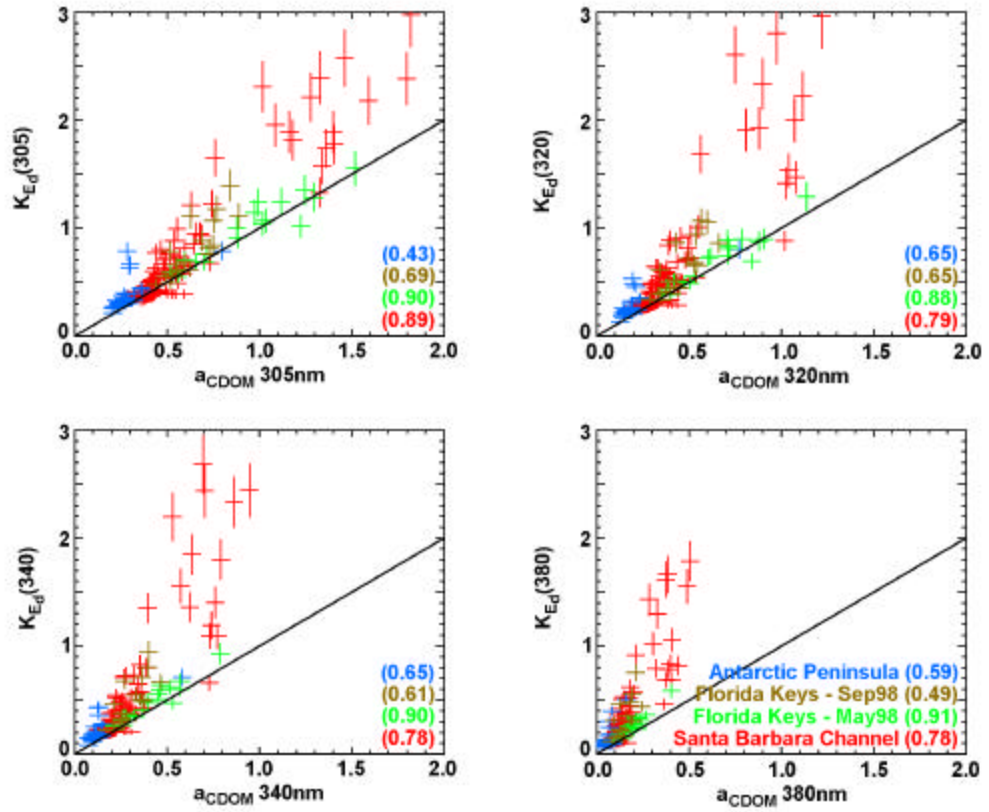
Figure 9: Absorption by chromophoric dissolved organic matter in surface water samples plotted versus average UV attenuation coefficients for the top 10m of the water column. The 1:1 line is also plotted. Correlation coefficients (r^2) are given in parentheses.

4. Spectral Characterization of a_{CDOM}

To better understand variability in UV attenuation in coastal waters, it is important to identify the major contributors to K(UV). At the time this document was prepared, only UV-visible absorption spectra of seawater CDOM, $a_{CDOM}(\lambda)$, and PRR/PUV diffuse attenuation coefficients, $K(\lambda)$, were available for all three regions.

Total seawater absorption is a measure of an inherent optical property (IOP) of the water (Preisendorfer, 1961), which means it is a property of seawater wholly dependent on the water composition and independent of the geometric shape of the radiance distribution of the light source at the time of data collection. Total seawater absorption can be expressed as the sum of absorption coefficients for each of the major components of seawater:

$$a(\lambda) = a_w(\lambda) + a_{CDOM}(\lambda) + a_p(\lambda)$$

$$a(\lambda) = \text{total absorption coefficient (m}^{-1})$$

$$a_w(\lambda) = \text{absorption coefficient for pure seawater (m}^{-1})$$

$$a_{CDOM}(\lambda) = \text{absorption coefficient for CDOM (m}^{-1})$$

$$a_p(\lambda) = \text{absorption coefficient for total particulate matter (m}^{-1})$$

Example absorption spectra for the different components are shown in Figure 2 for a seawater sample collected in the Antarctic.

Total seawater absorption is combined with photon loss due to scattering in the water column to determine total attenuation:

$$c(\lambda) = a(\lambda) + b(\lambda)$$

$$c(\lambda) = \text{total attenuation coefficient (m}^{-1})$$

$$a(\lambda) = \text{total absorption coefficient (m}^{-1})$$

$$b(\lambda) = \text{total scattering coefficient (m}^{-1})$$

In this equation, a(λ), b(λ) and c(λ) are all IOP's of the water column. The diffuse attenuation coefficient of seawater, K(λ), as measured by the PRR/PUV instrument is similar to c(λ), in that the magnitude of K(λ) is primarily due to absorption and scattering by seawater components. However, K(λ) is calculated from several measurements of solar radiation at different depths in the water column, making its value partially dependent on the geometric distribution of solar radiation at the depths, times and locations of the measurements; thus, by definition, K(λ) is an apparent optical property (AOP) of the water column (Preisendorfer, 1961). In this chapter, the focus of discussion will be on the absorption component of seawater attenuation. For more detailed discussions of the contribution of scattering to total seawater attenuation and relationships between K(λ) and seawater IOP's, the reader is referred to Kirk (1994b) or Mobley (1994).

Of the components of seawater contributing to a(λ) in the UV portion of the spectrum, water is generally the smallest contributor. While water is most often only a small contributor to UV attenuation, the absolute value of this contribution is a subject of controversy, with the few modern published values available varying over a factor of three (Figure 10). Absorption or attenuation coefficients reported in the literature were measured employing different laboratory techniques and measured waters were obtained through various purification and storage methods. To complicate matters further, very few published measurements have been made at the same UV wavelengths, making direct comparisons of methods difficult. Unfortunately, the most recent and most spectrally continuous values published in the 300-400nm range (Litjens *et al.*, 1999) are inconsistent in shape and magnitude with published visible water absorption values,

42

including average negative absorption values at a few wavelengths in the 360-500nm range, which raises concerns about the quality of their data.

Ultraviolet absorption by particulates can be broken down into two categories, absorption by phytoplankton and absorption by non-living particulates (Figure 2). The shape and magnitude of the particulate UV-visible absorption spectrum can vary considerably, depending on the concentrations of phytoplankton and non-living material and the presence or absence of UV-protective pigments, known as mycosporine-like amino acids (MAA's), in the phytoplankton population (Karsten *et al.*, 1998; Karentz *et al.*, 1991; Dunlap *et al.*, 1995; Shick *et al.*, 1992). The peak observed in the 310-360nm range in the example phytoplankton absorption from the Antarctic shown in Figure 2 is indicative of the presence of MAA's in the phytoplankton population.

The third category is chromophoric dissolved organic matter. Chromophoric dissolved organic matter differs from water and total particulates in that it absorbs extremely weakly in the visible portion of the spectrum and absorption increases approximately exponentially in the ultraviolet portion of the spectrum. As wavelength decreases in the ultraviolet to the UVB (280-320nm), a_{CDOM} often becomes the dominating contributor to seawater UV attenuation. These shorter UVB wavelengths are of particular interest because 280-320nm overlaps the absorption band of atmospheric ozone (Molina and Molina, 1986) and these shorter UV wavelengths have more energy per photon and higher potential to cause damage to organisms (i.e. Hunter *et al.*, 1981; Setlow, 1974; also Figure 1)

The generalized a_{CDOM} spectrum has historically been characterized by two parameters, the absorption coefficient at a chosen reference wavelength and the slope of a least-squares exponential curve fit (Bricaud *et al.*, 1981):

$$a_{CDOM}(\lambda) = a_{CDOM}(\lambda_r)e^{-S(\lambda-\lambda_r)}$$

λ = wavelength (nm)

λ_r = reference wavelength (nm)

S = slope parameter

For analyses presented in chapters 6 and 7, a reference wavelength of 305nm was chosen. There were two main criteria for choosing 305nm as the reference wavelength. First, since a_{CDOM} increases exponentially with decreasing wavelength, the wavelength of choice must be detectable for a large majority of samples collected. In the Antarctic, reliable detection was often reached between 320-350nm, limiting the range of potentially useful wavelengths to those ≤320nm. Second, 305nm corresponds to one of the PRR/PUV channels for which total seawater attenuation coefficients were calculated.

Slope parameters (S) for seawater and estuarine environments have been reported in the range 0.010-0.033nm^{-1} (Kirk, 1994b; Green and Blough, 1994; Vodacek *et al.*, 1997). For all study regions, a_{CDOM} spectra were recorded from 250-750nm, however the wavelength at which the reliable detection limit was reached ranged from approximately 320-600nm. Therefore, in order to compare slope parameters across space and time, the method used to calculate S must be free of biases. To explore the effect of using different wavelength ranges on calculated S values, a_{CDOM} spectra were separated into 10nm segments from 300-400nm and an S value was calculated for each 10nm interval. These S values calculated from 10nm intervals were then normalized to an S value calculated using all a_{CDOM} data in the 300-350nm wavelength range to remove the average slope from each spectrum.

Analysis of a_{CDOM} spectra indicates the magnitude of S depends on the wavelength range used to perform the exponential curve fit and S

generally decreases with increasing wavelength (Figure 11). There are a couple of scenarios, which may work individually or in combination to produce the observed decrease in S with increasing wavelength. Of course, as with any ecosystem variable, the a_{CDOM} spectrum measured at any one location and time represents a snapshot of the ever-changing complex balance of production or addition of material to the system and destruction or removal from the system.

First, changes in S with wavelength could arise from the existence of a combination of biogenous and terrigenous sources of CDOM in coastal waters. Chromophoric dissolved organic matter derived from marine materials, such as phytoplankton, generally have greater S values, while terrestrially-derived humic substances generally have smaller S values (Zepp and Schlotzhauer, 1981; Mopper *et al.*, 1995). As wavelength increases, the balance of components of CDOM doing the majority of absorption may shift from a more marine, high S source to a more terrestrial, low S source (Carder *et al.*, 1989). The differences between S values for terrestrial versus marine sources of CDOM were clearly seen in the Santa Barbara Channel – February 1998 dataset. In Figure 5, lower S values correspond to locations of brown sediment plume waters as observed on the February 9, 1998 SeaWiFS image.

Another possible reason for the change in S with wavelength is preferential photobleaching over time (Vodacek *et al.*, 1997). Kouassi and Zika (1992) have shown that when filtered seawater samples are irradiated with narrowband radiation, CDOM absorption decreases most around the wavelengths of irradiation. Since the shorter UV wavelengths are attenuated much more quickly in seawater than longer wavelengths, the bulk pool of seawater CDOM is exposed to more photons of longer UV

wavelengths over time, causing preferential photobleaching of a_{CDOM} at longer UV wavelengths.

Unfortunately, information concerning the origin, constituency and light exposure history of the a_{CDOM} seawater samples collected was not (and often cannot be) determined. Without data on the origin, constituency and light exposure history of the a_{CDOM} samples, the possible influences and interactions of the processes just discussed cannot be accurately assessed. In a hypothetical example, consider two parcels of surface water from fresh river plumes with identical a_{CDOM} spectra. One parcel is in a cloudy location with light to moderate winds and the terrestrial CDOM becomes mixed with the marine CDOM pool. The other parcel is in a clear-sky location with calm winds so the terrestrial CDOM pool remains isolated in the freshwater river plume, but becomes significantly photobleached. After a period of time, similar decreases in S might be observed in a_{CDOM} spectra of both parcels, however the processes causing the decreases in S were quite different.

Figure 11 is a plot of normalized a_{CDOM} 10nm interval S values for the Santa Barbara Channel and Florida Keys regions. The Antarctic dataset is not shown due to large data scatter arising from a_{CDOM} values being near or below the reliable detection limit and spectrophotometer noise problems. As can be seen in Figure 11, the average S value decreases 40-70% from 300 to 400nm, which is quite a significant decrease. Least-squares linear fits calculated from 10nm interval S values are also plotted in Figure 11, which are sufficient to account for first-order changes in S with wavelength. The scatter about the average and the linear fit is great at wavelengths >370nm. However, at these longer wavelengths, a_{CDOM} values are very small compared to the shorter UV wavelengths, thus the absolute change in calculated a_{CDOM} values are less

sensitive to changes in S. In contrast, small changes in S at shorter UV wavelengths can greatly change estimates of biologically effective doses of UV radiation (Figure 3).

In special cases, a_{CDOM} spectra show moderate bandwidth peaks or shoulders (hereafter referred to as "peaks") in the UV, which deviate significantly from the general exponential curve shape. Potential sources of these peaks include petroleum hydrocarbons in the Santa Barbara Channel and UV protective pigments, MAA's, produced by phytoplankton and other marine organisms (Karsten *et al.*, 1998; Karentz *et al.*, 1991; Dunlap *et al.*, 1995; Shick *et al.*, 1992). A few mechanisms through which MAA's could be transferred to the dissolved pool include death and decay of cells, breaking of cells during sloppy grazing or possible leakage of pigments across the cell wall, as has been observed in the laboratory for a red-tide dinoflagellate (Vernet and Whitehead, 1996). Under a vast majority of conditions, only integrated broadband UV absorption peaks resulting from the combination of absorption bands of individual MAA's can be detected in a_{CDOM} spectra. Concentrations of individual MAA's contributing to the observed broadband absorption peaks cannot generally be determined from a_{CDOM} spectra alone.

In Marguerite Bay, Antarctica (southeast corner of the LTER grid, south of Adelaide Island), MAA-like absorption peaks between 300-350nm were observed in twelve a_{CDOM} samples (six samples at two stations) in an area of dense phytoplankton bloom conditions (Figure 12). At these two stations, cell concentrations were dense enough to attenuate total visible irradiance (400-700nm) to 1% of the surface irradiance at depths between 10-15m. Similar peaks were also observed in a_{CDOM} samples of sea ice collected in Tickle Passage (east of Adelaide Island) and Matha Strait (north of Adelaide Island), where dense phytoplankton concentrations also

47

existed. However, the sea ice peaks could have been enhanced through laboratory processing as the sea ice was melted in order to filter out the particulate fraction.

In the Florida Keys, absorption peaks were not found in water column seawater samples. One sample was collected in the New Grounds region at the level of the benthic organisms, which purposefully contained a large quantity of gorgonian-produced mucous. This high-mucous a_{CDOM} sample also contained an MAA-like absorption peak similar to the one shown in Figure 12.

In the Santa Barbara Channel, two absorption peak wavelength regions have been encountered since May, 1997. One of those absorption peaks was in the range of 290-310nm and the other was similar to the MAA-like absorption peak between 300-350nm. However, patterns indicating the potential sources of these peaks have not been found and, at times, there may be contamination issues such as petroleum hydrocarbon residues remaining in the sample bottle between samplings. While precautions were taken to avoid such contamination, it could not always be avoided and was not routinely documented in the early days of a_{CDOM} sampling.

There is currently no method to predict when and where moderate bandwidth UV peaks occur. However, these peaks are of paramount importance in estimating biologically effective UV doses for marine organisms since they absorb in the wavelength range often responsible for the largest portion of the weighted UV dose (Figures 1 and 3).
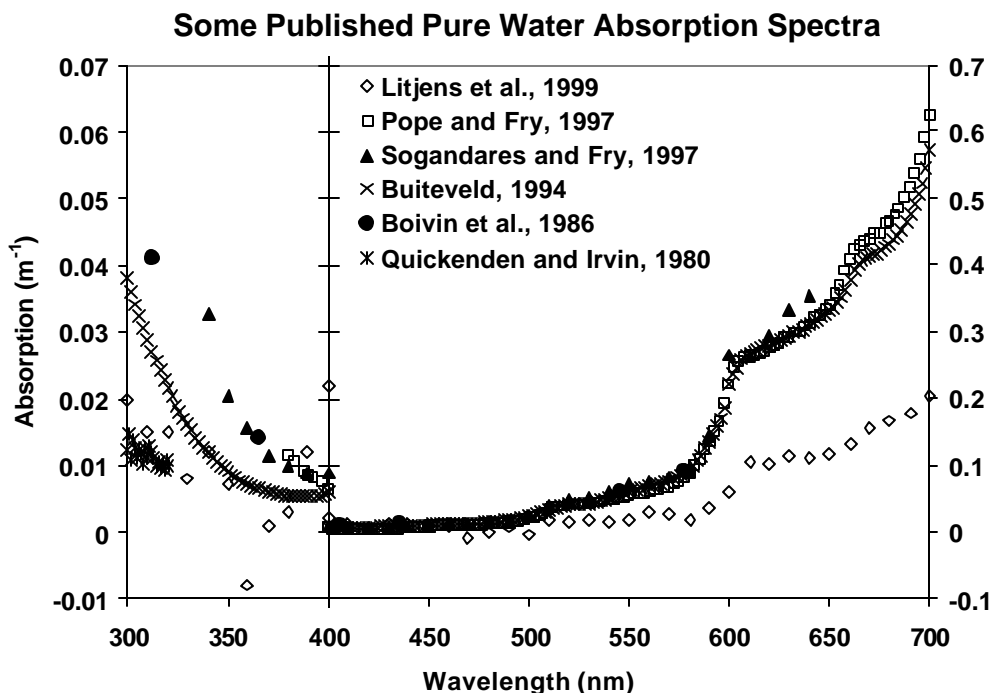
Some Published Pure Water Absorption Spectra

Figure 10: Some example pure water absorption spectra from recent literature. The references for each dataset are given in the plot legend. Wavelengths shorter than 400nm are plotted using the scale on the left and wavelengths longer than 400nm are plotted using the scale on the right. The values of Litjens *et al.*, 1999 were determined using the pathlength subtraction method using a single long-pathlength (1.5m) spectrophotometer cell. Pope and Fry (1997) values were determined using an integrating cavity absorption meter. Sogandres and Fry (1997) values were determined using a scattering insensitive photothermal method. Buiteveld (1994) did not make any measurements, but rather recommended a spectrum based on curve fits and other adjustments to previously published spectra. The values of Boivin *et al.*, 1986 were measured using a single long-pathlength cell (50.5cm) and include some scattering. Quickenden and Irvin (1980) values were calculated using the pathlength subtraction method using combinations of short-pathlength (1, 5 and 10cm) spectrophotometer cells.
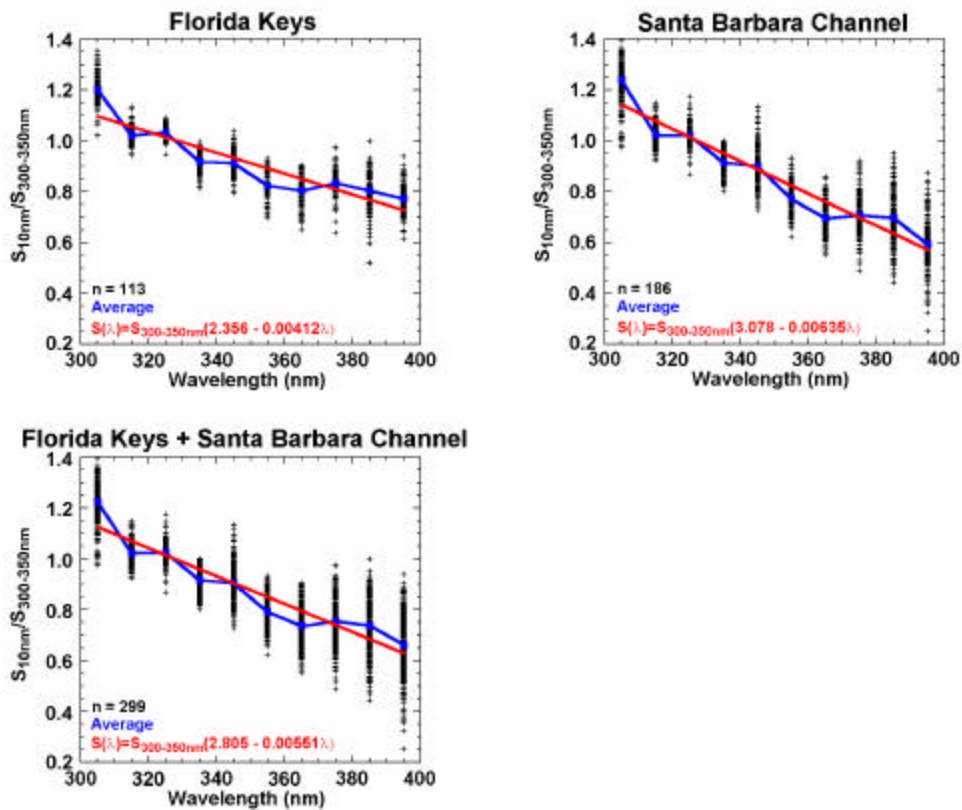
Figure 11: Slope parameters calculated for 10nm intervals between 300-400nm normalized to the slope parameter calculated using a_{CDOM} data between 300-350nm. For clarity, plot symbols are plotted at the center wavelength of each 10nm interval. A few spectra with distinct deviations from an exponential curve shape and high sediment river plume waters were excluded to obtain typical seawater conditions. Average values are plotted in blue and the least-squares fit line calculated using the average values are plotted in red. The number of samples used (n) and the equations for calculating the wavelength-dependent slope parameter using the least-squares linear fits are given in the bottom of each plot.
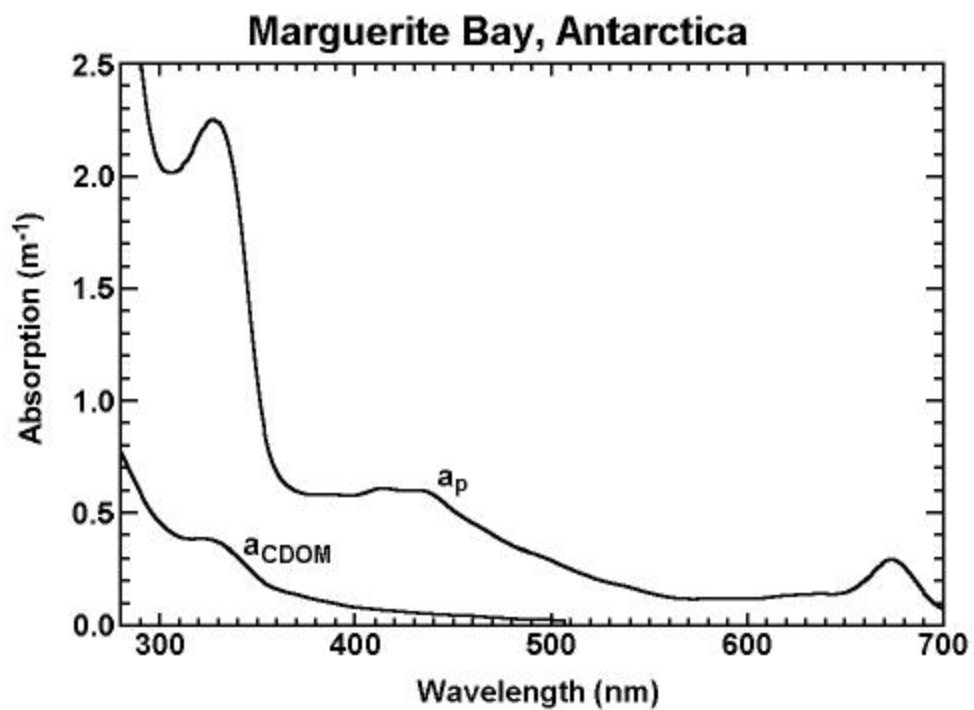
Figure 12: Particulate and dissolved absorption spectra for a surface sample collected in Marguerite Bay, Antarctica showing evidence of UV-protective pigments in the pool of chromophoric dissolved organic matter.

5. Contribution of a_{CDOM} to K(UV)

As mentioned earlier, in order to understand variability in total UV attenuation, it is important to understand the variability in the dominant components controlling UV attenuation. Chromophoric dissolved organic matter is one of the dominant absorbers of UV radiation in seawater. For this analysis, surface a_{CDOM} values were plotted against PRR/PUV attenuation coefficients at 305, 320, 340 and 380nm calculated from the top 10m of data in each cast (Figure 9).

A couple of things should be kept in mind when interpreting data presented in this section. First, since a_{CDOM} values were 240ml samples from surface water and K(UV) were calculated from all data collected in the top 10m, a_{CDOM} occasionally exceeds K(UV) in situations where there is a relatively thin surface feature. For example, during the Florida Keys – May 1998 cruise, there was one datapoint where a_{CDOM} exceeded K(UV) and this datapoint corresponded to a station where there was a large surface algal mat. Second, a_{CDOM} values were scanned using a 4nm slit width on the spectrophotometer, measuring the transmission of lamp irradiance through a 10cm sample of filtered seawater and the UV channels of the PRR/PUV have 10-15nm bandwidths, measuring the transmission of solar radiation through 10m of seawater. The shape of the solar UV spectrum in seawater changes greatly between the surface and 10m, with shorter UV wavelengths being attenuated most rapidly, thus K(UV) becomes more and more weighted by longer UV wavelengths as depth increases (Patterson *et al.*, 1996). The change in shape of the lamp spectrum across a 10cm pathlength is much less in comparison and the a_{CDOM} value is much more true to the quoted wavelength.

A few general observations can be made from Figure 9. First, the proportion of K(UV) attributable to a_{CDOM} decreases with increasing wavelength as demonstrated by datapoints clustering further away from the 1:1 line with increasing wavelength (also Table 3). Second, the correlation between a_{CDOM} and K(UV) generally decreases with increasing wavelength. This is indicative of shifting control of K(UV) variability from CDOM to particulate matter with increasing wavelength. Third, scatter between a_{CDOM} and K(UV) increases as the magnitudes of these values increase. The largest scatter between a_{CDOM} and K(UV) were found in the plume waters sampled in the Santa Barbara Channel in February, 1998 (all $a_{CDOM}(305)$ values >0.7m^{-1} in Figure 9).

The general trends just mentioned did not hold for the Florida Keys – May, 1998 cruise dataset. Contribution of a_{CDOM} to K(UV) decreases with increasing wavelength keeping with the general trend, however, the average a_{CDOM}/K(UV) ratios in the Florida Keys – May, 1998 cruise were much higher than in the other regions (Table 3). The correlation between a_{CDOM} and K(UV) remained very high (r^2>0.88) for all four UV wavelengths and the average a_{CDOM}/K(UV) values were >0.77 for all UV channels, indicating a_{CDOM} maintained dominance over K(UV) variability throughout the UVB and UVA. However, as was discussed earlier, K(UV) did not correlate well with K(412) (Table 2), so this dominance does not appear to extend into the blue portion of the spectrum. Since 412nm is within the strong chlorophyll absorption band of phytoplankton, it appears that while a_{CDOM} dominated UV attenuation during this cruise, phytoplankton most likely dominated K(412) resulting in the low correlation between K(UV) and K(412).

The Antarctic Peninsula region also deviated a little from the general trends. This region had the lowest a_{CDOM} and K(UV) values as well as the

lowest correlation between a_{CDOM} and K(UV). Low a_{CDOM} and K(UV) values were expected due to the relative lack of significant terrigenous input into the water column. Low correlation between a_{CDOM} and K(UV) may be an indicator that variability in K(UV) was dominated by particulate matter. This last statement is made somewhat hesitantly, though, since K(UV) values were small and a majority of the variability in a_{CDOM} values in the Antarctic were within the noise range of the spectrophotometer.

Table 3: Average ratios of a_{CDOM} to K(UV) for the different study regions.

Dataset	$\dfrac{a_{CDOM}(305)}{K(305)}$	$\dfrac{a_{CDOM}(320)}{K(320)}$	$\dfrac{a_{CDOM}(340)}{K(340)}$	$\dfrac{a_{CDOM}(380)}{K(380)}$
Florida Keys May 1998	0.95	0.93	0.86	0.77
Florida Keys Sept. 1998	0.83	0.76	0.68	0.56
Santa Barbara Channel Core Cruises	0.93	0.87	0.76	0.60
Santa Barbara Channel February 1998	0.70	0.58	0.51	0.41
Antarctic Peninsula	0.81	0.74	0.64	0.55

6. Spatial Variability in K(UV) and a_{CDOM}

In the open ocean, seawater attenuation can be expected to correlate mainly with the biological activities of the water column as the water depths are sufficiently deep to avoid sediment resuspension events and the locations are sufficiently far from terrigenous inputs from large landmasses. Coastal water ecosystems are more complex than open ocean ecosystems in that nearby landmasses and the bottom composition of shallow shelves can have significant impacts on the ecosystem. Patterns of spatial variability in UV attenuation and UV absorption by CDOM were analyzed using K(UV) values calculated from the top 10m of data in each PRR/PUV cast, surface CDOM absorption at 305nm and the a_{CDOM} slope parameter (S) calculated from the a_{CDOM} spectrum in the 300-350nm range. Profile a_{CDOM} samples were also collected at various stations in the three regions, however most profiles did not show a significant detectable change with depth, so these will not be discussed.

Ultraviolet attenuation coefficients are expected to be higher during periods of high particulate load. Terrigenous sediment input from storm-water runoff would be one source of UV-attenuating particulates and are generally accompanied by increased input of land-derived UV-absorbing dissolved organic matter as well. During phytoplankton bloom conditions, as one might observe after spring upwelling events, which introduce large quantities of nutrients into the euphotic zone, UV attenuation by phytoplankton and detrital particles formed as the bloom cells die and decay would be expected to increase. Accordingly, these high particle load situations would also be expected to have higher UV absorption by chromophoric dissolved organic matter. For these reasons, spatial patterns of the a_{CDOM} slope parameter are not necessarily expected to

follow in step with spatial patterns of a_{CDOM} absorption magnitudes or K(UV). Land-derived CDOM tends to have lower S values, while marine-derived CDOM tends to have higher S values (Zepp and Schlotzhauer, 1981; Mopper *et al.*, 1995), therefore, spatial patterns of S would be expected to relate more to the relative contribution of land- versus marine-derived material. However, CDOM is modified by photobleaching and microbial processing (Kouassi and Zika, 1992; Miller and Moran, 1997; Lindell *et al.*, 1995), complicating the interpretation of both a_{CDOM} and S value spatial and temporal patterns. Since the UV history of the samples collected and microbial activity were not measured during these studies, the overall impact of these processes on a_{CDOM} and S values cannot be commented upon.

To put the three study regions into perspective, the regions were compared against one another based on bulk statistical parameters, which are summarized in Table 4. The waters of the Antarctic Peninsula were the most UV transparent of the three regions. The Antarctic also had the lowest a_{CDOM} values with average $a_{CDOM}(305)$ in the Antarctic 30-74% of the averages of the other two regions. This was expected due to the much decreased terrestrial influence and deep water depths for a large portion of the LTER grid, making this a more open ocean type regime.

What was not expected was the slightly higher UV attenuation in the Florida Keys on average compared to the Santa Barbara Channel (Table 4). The range of $a_{CDOM}(305)$ in the Florida Keys was also somewhat surprising, with some values during the May 1998 cruise as high as values encountered in the fresh river sediment plume sampled in the Santa Barbara Channel during February 1998. These results seemed contradictory to initial preconceptions of tropical reef locations as being pristine, optically clear waters. While the following cannot be proven with

the data collected, one possible reason for the high UV attenuation in the Florida Keys compared to the Santa Barbara Channel is that the Florida Keys study region is bordered to the north by a wide shallow shelf (depth <20m) extending from the wetland habitats of southern Florida. While wetland habitats can be good filters for terrigenous particulates, dissolved substances are allowed to pass through. Unlike southern Florida, which experiences some degree of storm activity throughout the year, storm activity in the Santa Barbara Channel region is generally restricted to the winter storm season from November through March. Consequently, terrigenous input of dissolved substances into the Santa Barbara Channel is also rather restricted to the winter storm season, and then most of the discharge is released by the Santa Clara and Ventura Rivers at the far east corner of the Channel (Mertes *et al.*, 1998).

6.1. Santa Barbara Channel

Considering variability within regions, the Plumes and Blooms core transect lies in a very complex area of the Santa Barbara Channel. The transect is fairly centered longitudinally in the Channel, where cold waters entering from the west meet relatively warmer waters entering from the southeast. With the different circulation patterns in the Channel, the transect can consist entirely of warmer waters from the southeast during flood west conditions, entirely of colder waters from the northwest during flood east conditions, or warmer waters at more northern transect stations and colder waters at more southern transect stations during upwelling, relaxation, cyclonic and propagating cyclones circulation patterns (Harms and Winant, 1998). From AVHRR (Advanced Very High Resolution Radiometer) sea surface temperature snapshots collected near the times

of Plumes and Blooms cruises, all of these regimes as well as transitional regimes were sampled during the time period studied.

Some of the stations along the transect have localized influences, which do not generally affect the other stations along the transect. For the following discussion, keep in mind that stations along the Plumes and Blooms transects are numbered from 1 to 7 from north to south (Figure 4c). Station 1 is influenced by outflow from Goleta Slough, including occasional discharge from a water treatment plant located near the mouth of the Slough. An area of natural oil seepage is located between stations 1 and 2. Depending on local winds and surface currents, the extent of the surface oil slick can occasionally reach one of these two stations during any particular cruise. Under most current regimes, station 7 is located immediately downcurrent from Santa Rosa Island. Thus, station 7 is generally highly influenced by runoff from the island and the productive benthic ecosystem on the shallow northwest shelf of the island. While stations 1 and 7 are in relatively shallow water (50-70m) near land, stations 2-6 are in the deep basin with bottom depths >200m, away from the immediate land/shelf influences.

When K(UV), a_{CDOM} and S(300-350) were plotted and compared to AVHRR sea surface temperature imagery, similar patterns often appeared (Figure 13). In general, the colder waters from the west were associated with higher K(UV) and a_{CDOM} and lower S(300-350) than the warmer waters from the southeast. Visual analysis was confirmed by correlation analysis using all deep water stations (i.e. excluding stations 1 and 7) sampled during core cruises and the October '97 cruise. Correlation coefficients (r^2) for K(UV), a_{CDOM} and S(300-350) plotted versus CTD sea surface temperature was generally greater than 0.5. Other than this temperature correlation, there were no consistent correlations with any of the other

biological, physical or chemical datasets routinely collected on the Plumes and Blooms cruises.

On some individual cruises, however, there were some significant correlations ($r^2 > 0.7$) with other datasets. Specifically, during the October 1997 cruise, K(UV) correlated with chlorophyll *a* and phaeopigments, but this correlation did not hold true for a_{CDOM}. In contrast, during the February 1998 cruise, K(UV) and a_{CDOM} parameters highly correlated with datasets relating to the existence of sediment plume waters, such as salinity, transmissometer and nutrient measurements. Spatial patterns of K(UV), a_{CDOM} and S(300-350) matched remarkably well to the plume patterns seen on the February 9, 1997 SeaWiFS visible composite satellite image (Figure 5).

6.2. Florida Keys

Aside from frequently used shipping channels and harbors, the general patterns observed during the Florida Keys cruises can be explained in terms of water mass influences. While currents were not measured during these cruises, patterns in K(UV) and a_{CDOM} match scenarios described by Lee *et al.* (1994). There is an area of very shallow waters and occasional parcels of land which extends due west from Key West to the Dry Tortugas. Stations on or north of these shallows displayed higher K(UV) and a_{CDOM} than reefs to the south of Key West (Figure 14). To the north, water masses are characterized by a shallow shelf ecosystem (depths <20m) extending from the organically rich wetlands of the Florida Everglades. To the south of the study region, the shelf drops off rapidly to depths >1000m, with prevailing eastward current flow of Gulf of Mexico waters through the South Florida Straits.

During the Florida Keys May 1998 cruise, the latitudinal differences in K(UV) and a_{CDOM} values were extreme. The patterns matched general AVHRR sea surface temperature patterns on images collected a few days prior to the cruise, with a localized area of unusually cold waters approaching 20°C in the Dry Tortugas (Figure 14). This scenario is described by Lee *et al.* (1994) as the cold cyclonic Tortugas Gyre, which keeps CDOM-rich shelf waters in the Dry Tortugas area. When K(UV) and a_{CDOM} values were compared to measured temperature profiles, these values correlated with bottom water temperatures, not sea surface temperatures. This discrepancy can be explained by the development of well stratified waters during the calm, clear conditions during the beginning of the cruise, allowing surface waters to warm while a few meters below, the water maintained its cold temperature (data not shown). By early June 1999, evidence of cold cyclonic circulation in the region had disappeared from AVHRR imagery.

During the Florida Keys September 1998 cruise, the general patterns remained the same except for in the Dry Tortugas (Figure 14). In this scenario, the patterns in the Dry Tortugas suggest a strong influence by Gulf of Mexico waters from the west and/or south. The Tortugas Gyre was absent during this cruise. The Gulf of Mexico water is expected to be warm and CDOM-poor compared to the shelf water. The only high K(UV) and a_{CDOM} samples found in the Dry Tortugas during the September 1998 cruise were in the approach channel to the Fort Jefferson Harbor, which had experienced a great deal of boat traffic and turbulence due to increased tourist activity during the Labor Day holiday. While most areas appear to be under the influence of CDOM-poor Gulf waters, the New Grounds area maintains higher K(UV) and a_{CDOM} values indicative of shelf-water influence. During the September 1998 cruise, waters were generally

warm and well-mixed in the study region, with several tropical storms passing through the eastern Gulf during this time period and cloud-free satellite imagery could not be obtained for this cruise.

6.3. Antarctic Peninsula

In the Antarctic, the spatial patterns were fairly simple. K(UV) and a_{CDOM} were highest south of Adelaide Island in Marguerite Bay, moderate at nearshore stations and decreased as distance from shore increased (Figure 15). Due to spectrophotometer problems and low a_{CDOM} values, reliable a_{CDOM} S(300-350) could not always be calculated. However a clearly discernable difference could be distinguished between Marguerite Bay and vicinity and the rest of the LTER grid, with S(300-350) much lower at about 0.011-0.012nm^{-1} compared to values generally above 0.020nm^{-1} for the rest of the LTER grid. These spatial patterns coincided with spatial patterns visible on a cruise composite satellite-derived image of primary production (Ray Smith and Heidi Dierssen, personal communication; Figure 15). Highest primary productivity was found in Marguerite Bay; otherwise, general patterns showed moderate primary productivity nearshore, which decreased offshore. Similar patterns in chlorophyll and primary productivity have been observed by Smith *et al*. (1996).

While visual patterns in K(UV) and a_{CDOM} were similar to patterns observed in chlorophyll and primary productivity, there were no strong quantitative correlations between K(UV) or a_{CDOM} parameters and chlorophyll. However, such a correlation would not necessarily be expected due to the fact that there is little terrestrial input of CDOM to Antarctic waters, leaving the death and senescence of phytoplankton as the major source of CDOM. Therefore, variability in a_{CDOM} might not be expected to coincide with variability in chlorophyll, but rather variability in

a_{CDOM} would more likely be expected to correlate with variability in chlorophyll at some time in the recent past. Data were not available to check for time-lagged correlations between chlorophyll and a_{CDOM}.

Table 4: Bulk statistical parameters for UV attenuation, CDOM absorption and the a_{CDOM} slope parameter (S) in the Florida Keys (FK), Santa Barbara Channel (SBC) and west Antarctic Peninsula (WAP). Average values listed in gray indicate the full dataset was not available for statistical calculations due to instrument detection limits being reached. ND = not detectable.

|	FK-May98	FK-Sep98	SBC-Oct97	SBC-Feb98	SBC-Core	WAP
Minimums						
$a_{CDOM}(305)$	0.52	0.44	0.29	0.42	0.33	0.21
$a_{CDOM}(320)$	0.36	0.29	0.20	0.29	0.23	0.13
$a_{CDOM}(340)$	0.22	0.17	0.12	0.19	0.15	ND
$a_{CDOM}(380)$	0.09	0.08	0.05	0.10	0.06	ND
$K_{Ed}(305)$	0.55	0.48	0.32	0.52	0.35	0.21
$K_{Ed}(320)$	0.38	0.34	0.22	0.42	0.26	0.13
$K_{Ed}(340)$	0.26	0.22	0.15	0.33	0.18	0.08
$K_{Ed}(380)$	0.11	0.12	0.07	0.21	0.09	0.05
S(300-350)	0.0185	0.0183	0.0187	0.0169	0.0159	0.0110
Averages ± Standard Deviation						
$a_{CDOM}(305)$	0.92 ±0.29	0.64 ±0.13	0.38 ±0.05	0.91 ±0.43	0.44 ±0.07	0.28 ±0.09
$a_{CDOM}(320)$	0.65 ±0.21	0.46 ±0.10	0.27 ±0.03	0.68 ±0.34	0.33 ±0.06	0.19 ±0.10
$a_{CDOM}(340)$	0.42 ±0.14	0.30 ±0.08	0.17 ±0.03	0.48 ±0.24	0.22 ±0.05	0.13 ±0.08
$a_{CDOM}(380)$	0.20 ±0.07	0.15 ±0.05	0.09 ±0.02	0.25 ±0.13	0.11 ±0.03	0.06 ±0.02
$K_{Ed}(305)$	0.97 ±0.30	0.81 ±0.27	0.38 ±0.03	1.35 ±0.70	0.49 ±0.12	0.36 ±0.13
$K_{Ed}(320)$	0.70 ±0.23	0.64 ±0.24	0.28 ±0.03	1.18 ±0.76	0.39 ±0.13	0.27 ±0.12
$K_{Ed}(340)$	0.49 ±0.17	0.48 ±0.21	0.20 ±0.03	1.03 ±0.71	0.31 ±0.12	0.21 ±0.11
$K_{Ed}(380)$	0.26 ±0.10	0.31 ±0.17	0.11 ±0.02	0.68 ±0.46	0.20 ±0.10	0.14 ±0.09
S(300-350)	0.0222 ±0.0016	0.0213 ±0.0022	0.0219 ±0.0018	0.0187 ±0.0014	0.0203 ±0.0026	0.0236 ±0.0041
Maximums						
$a_{CDOM}(305)$	1.52	0.89	0.46	1.82	0.68	0.80
$a_{CDOM}(320)$	1.14	0.66	0.32	1.39	0.51	0.77
$a_{CDOM}(340)$	0.79	0.47	0.22	0.98	0.35	0.58
$a_{CDOM}(380)$	0.40	0.24	0.12	0.51	0.18	0.16
$K_{Ed}(305)$	1.55	1.39	0.44	>3.00	0.95	0.79
$K_{Ed}(320)$	1.29	1.07	0.34	>3.00	0.93	0.80
$K_{Ed}(340)$	0.93	0.94	0.25	>3.00	0.83	0.71
$K_{Ed}(380)$	0.58	0.75	0.15	1.78	0.62	0.51
S(300-350)	0.0249	0.0258	0.0256	0.0227	0.0258	0.0331
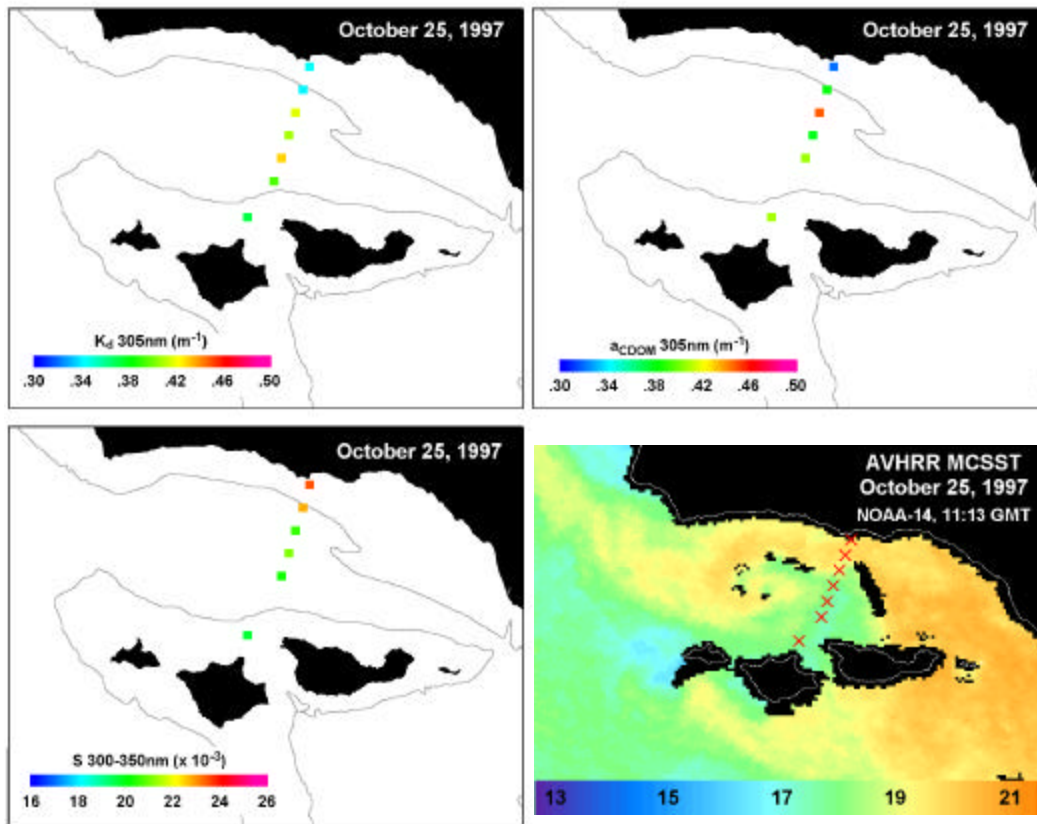
Figure 13: Top 10m ultraviolet attenuation and surface CDOM absorption at 305nm at Plumes and Blooms Stations on October 25, 1997. The a_{CDOM} slope parameter calculated using data in the 300-350nm range is also plotted. Patterns seen in the data collected across the Plumes and Blooms transects were similar to those seen on AVHRR Multi-Channel Sea Surface Temperature (MCSST) imagery collected on the same day. The AVHRR image was obtained from the UCSB/ICESS AVHRR web page (http://www.icess.ucsb.edu/avhrr/Channel_gifs/1997-10-25.1113.noaa-14.n.mcsst.SC1km.SBchnl.gif). The 200m bathymetry contour is plotted for reference. Note a change in scales between Figures 5 and 13.
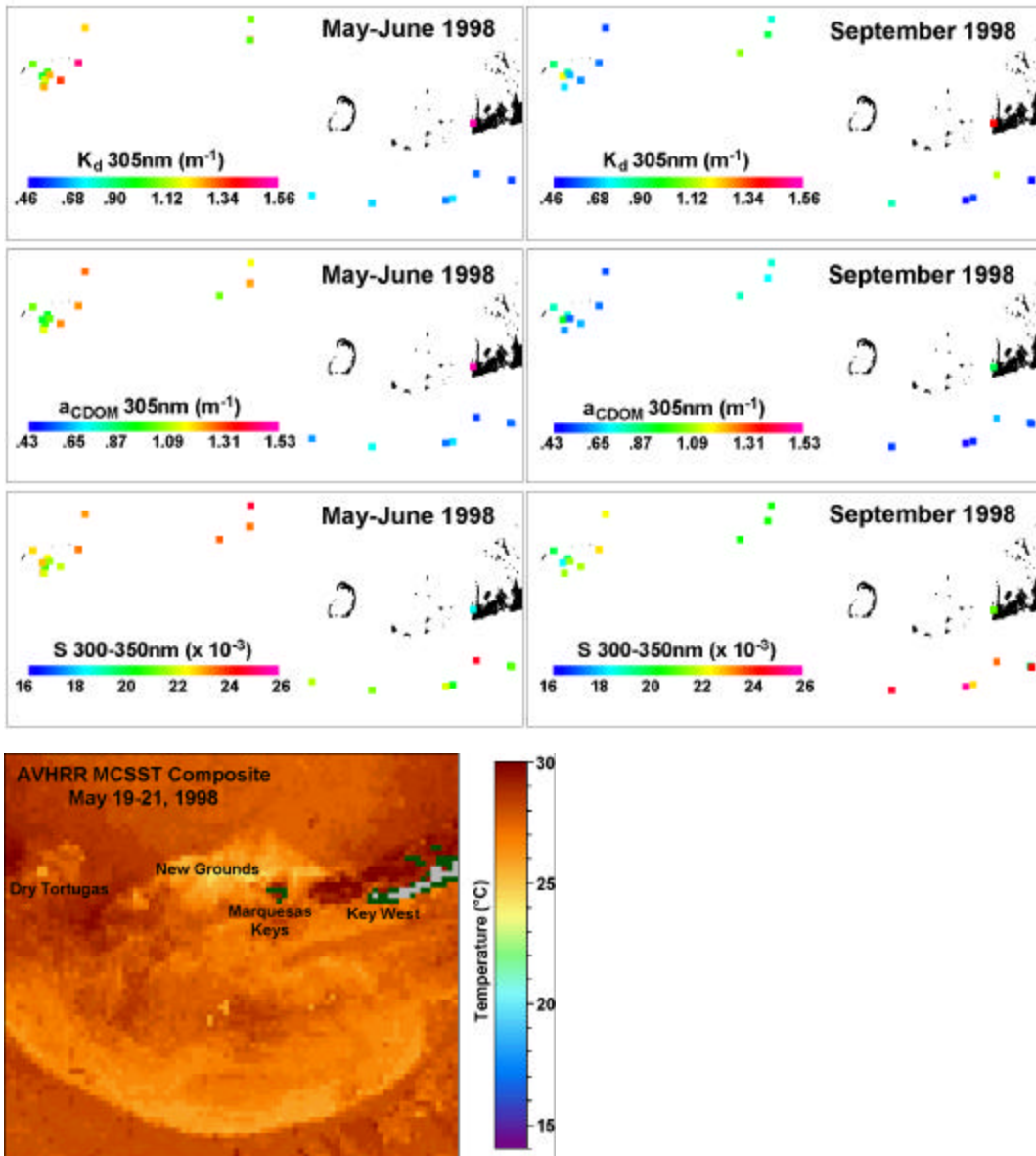
Figure 14: Ultraviolet attenuation at 305nm, a_{CDOM} at 305nm and S(300-350nm) for the two Florida Keys cruises. Spatial patterns during the May-June 1998 cruise were similar to 3-day composite AVHRR MCSST imagery obtained from the Johns Hopkins University Applied Physics Laboratory web page (http: //srbdata.jhuapl.edu/d0043/avhrr/gm/averages/98may/gm_98may21_2116_multi.gif). Clear sky imagery was not available for the September 1998 cruise. Geographical references are shown in Figure 4b.
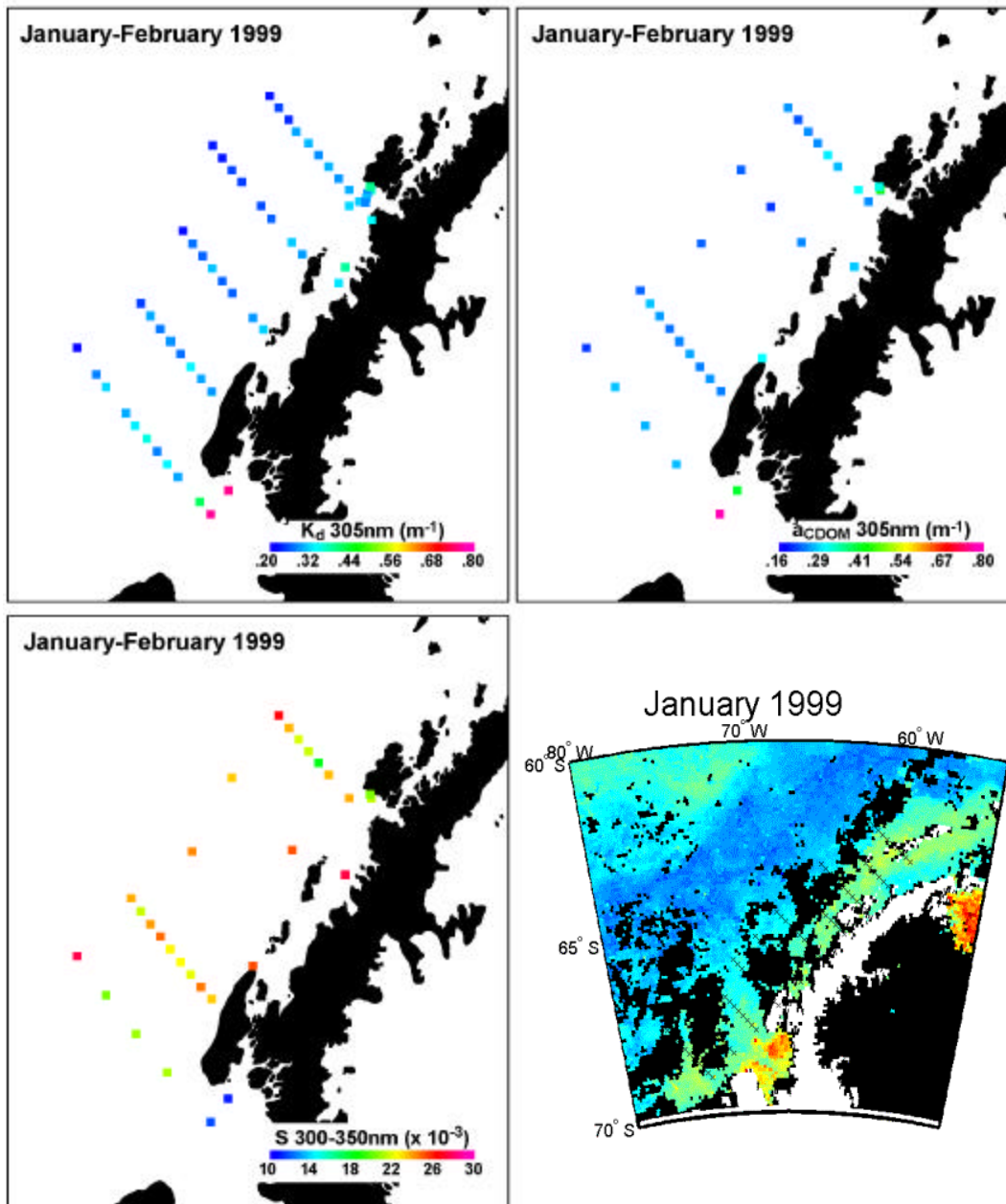
Figure 15: Ultraviolet attenuation at 305nm, a_{CDOM} at 305nm and S(300-350nm) for the west Antarctic Peninsula in January 1999. Spatial patterns observed coincide with general spatial patterns shown on a cruise-composite image of SeaWiFS-derived primary productivity shown at bottom, right (Ray Smith and Heidi Dierssen, personal communication). SeaWiFS primary productivity is plotted on a relative scale from blue (low primary productivity) to red (high primary productivity).

7. Temporal Variability in K(UV) and a_{CDOM}

A couple of different time scales were sampled amongst the three study regions. In the Florida Keys, short time scale variability was explored by sampling the same station 4-6 times over about a 24 hour period. In the Santa Barbara Channel and Antarctic Peninsula regions, a few stations were sampled multiple times, depending on weather and sea conditions, over a period of several months.

As mentioned for spatial variability, K(UV) and a_{CDOM} would be expected to be higher during periods of higher land-derived inputs, such as during storm events and during phytoplankton blooms spawned from the introduction of nutrients into the region's surface waters during events such as upwelling. However, the retention time for high K(UV) and a_{CDOM} after periods of high dissolved and particulate loads depends on surface currents, which laterally remove matter from the local region, and the speed at which photochemical breakdown and microbial processing of CDOM occurs. Temporal patterns in the a_{CDOM} slope parameter would indicate the complex balance of quantity and source of CDOM input, lateral movement of CDOM in or out of the local region through surface currents, photochemical breakdown (photobleaching), and microbial processing.

7.1. Santa Barbara Channel

In the Santa Barbara Channel, the Plumes and Blooms transect was sampled approximately 1-2 times per month, weather permitting, from September 1997 through July 1998. While the temporal variability between the seven core Plumes and Blooms stations in the Santa Barbara Channel appears quite complex, a common seasonal pattern is displayed. To show the overall temporal pattern more clearly, averages of $K_{E_d}(305)$, $a_{CDOM}(305)$

and S(300-350) from the mid-Channel stations (Plumes and Blooms stations 2-6) were calculated for each cruise and plotted as a function of time (Figure 16). During the fall and early winter, $K_{E_d}(305)$ and $a_{CDOM}(305)$ were low and S(300-350) was high. As winter storm activity increased, $K_{E_d}(305)$ and $a_{CDOM}(305)$ increased and S(300-350) decreased, indicative of land-derived materials entering the ecosystem during this period. Values returned to pre-storm season values in summer 1998 after the end of the winter storm period.

In Figure 16, three peaks in $K_{E_d}(305)$ and $a_{CDOM}(305)$ occur within the overall seasonal pattern, which are associated with decreases in S(300-350). The first peak in February 1998 is associated with intense storm activity and flooding, with large amounts of terrestrial CDOM and particulates, indicated by lithogenic silica concentrations, entering the Channel. The immense input of terrigenous materials could be seen on the February 9, 1998 SeaWiFS visible composite image (Figure 5). The peaks in late April and late May/early June coincide with upwelling conditions and are associated with high nutrient and chlorophyll *a* values (Figure 16). It is important to note that El Niño weather and circulation patterns dominated during the study period and storms continued in this region through the beginning of June. Normally, storms and storm runoff is confined to the months of November through March, thus the timing of the patterns observed would not necessarily be expected in a typical year.

7.2. Florida Keys

During each of the May 1998 and September 1998 cruises in the Florida Keys, 2-3 stations with depths between 7-10m were chosen for tidal cycle sampling. Water samples were collected 4-6 times during an

approximate 24 hour period, with collection times chosen to coincide with high tide, falling tide, low tide and rising tide. Due to logistical constraints, profile Hydrolab and light casts were only collected once or twice during the tidal cycle sampling periods. However, a Datasonde was deployed for continuous temperature, dissolved oxygen and pH measurements at a depth of 1m above the reef bottom.

While some reefs experienced significant tidal currents, which can cause sediment resuspension or move water masses of different compositions over the local reef at different times during the tidal cycle, there were no consistent patterns in a_{CDOM} or S(300-350) with water mass indicators, such as temperature (data not shown), or tidal state (Figure 17). There were also no consistent patterns with time of day, which one might see if there were daily cycles of CDOM production and/or degradation and destruction.

While short-term temporal patterns could not be explained with the data collected, there were some significant changes in the magnitude of a_{CDOM} over the 24-hour periods sampled. For the reefs sampled, $a_{CDOM}(305)$ values varied by up to $0.27m^{-1}$ and S(300-350) values varied by up to $0.005nm^{-1}$ over the sampling period. These magnitudes of variability are of particular concern for the biologist calculating biologically effective UV doses for the reef corals, as was discussed in Chapter 1. Biologically effective doses were calculated using five a_{CDOM} spectra from the May 1998 Dry Tortugas tidal cycle sampling as the sole attenuator of surface UV irradiance in the example shown in Figure 3. Resulting biologically effective doses varied about 20% depending on the a_{CDOM} spectrum used, which is quite a significant amount of variability for such a short time period.

7.3. Antarctic Peninsula

In the Antarctic, the Palmer area stations B and E (Figure 4c inset) were sampled on 19 occasions when weather and the cruise schedule permitted between October 1998 and March 1999. Due to low a_{CDOM} values and spectrophotometer noise problems, the variability in a_{CDOM} values was not sufficient to make reliable comparisons between temporal patterns in a_{CDOM} parameters and temporal patterns in ancillary datasets.

From visual analysis of plots of top 10m $K_{E_d}(305)$, surface chlorophyll *a* and percent transmission from the CTD transmissometer at 1m depth, some pattern similarity can be seen (Figure 18). In general, there was much less variability over time in all variables sampled at station E. Temporal changes in $K_{E_d}(305)$ at station E often follow the shape of temporal changes in surface chlorophyll *a*. In contrast, $K_{E_d}(305)$ at station B patterns generally match closer with percent transmission at 1m. There were two periods of high UV attenuation at station B, which coincide with increased water column particulates. The high $K_{E_d}(305)$ values in early January can be attributed to a phytoplankton bloom, as indicated by high chlorophyll *a* values. However, the high $K_{E_d}(305)$ after mid-February occurs during a period of low chlorophyll *a* values, but high particulate matter as indicated by a decrease in percent transmission. Filters from water samples collected during the last few weeks of the season were noticeably gray, indicating the source of particulates during this time period was most likely glacial flour.
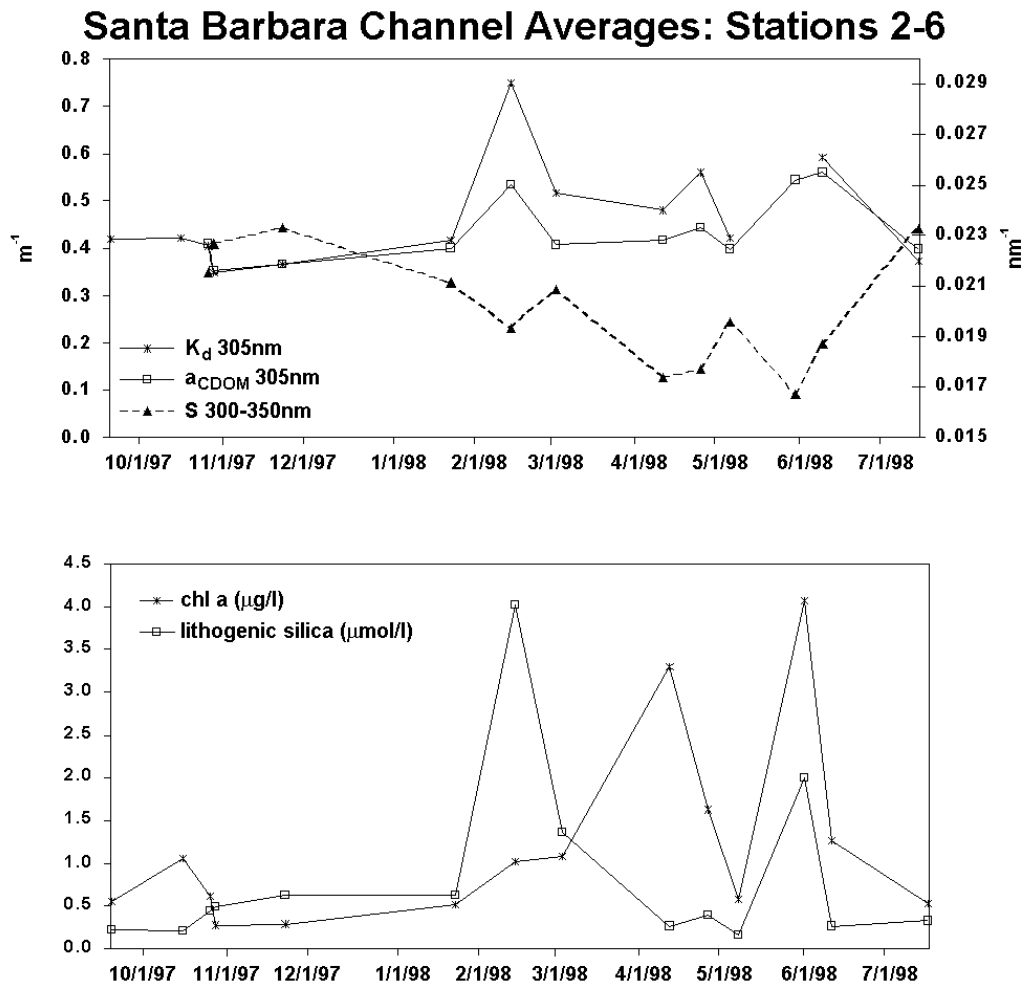
Figure 16: Average UV attenuation at 305nm, a_{CDOM} at 305nm and S(300-350nm) plotted versus time for the Santa Barbara Channel deep water stations (Plumes and Blooms stations 2-6). Average chlorophyll *a* and lithogenic silica are also plotted to show that the major features observed in the optical time series coincide with either phytoplankton blooms (high chlorophyll *a*) or high terrigenous input (high lithogenic silica).
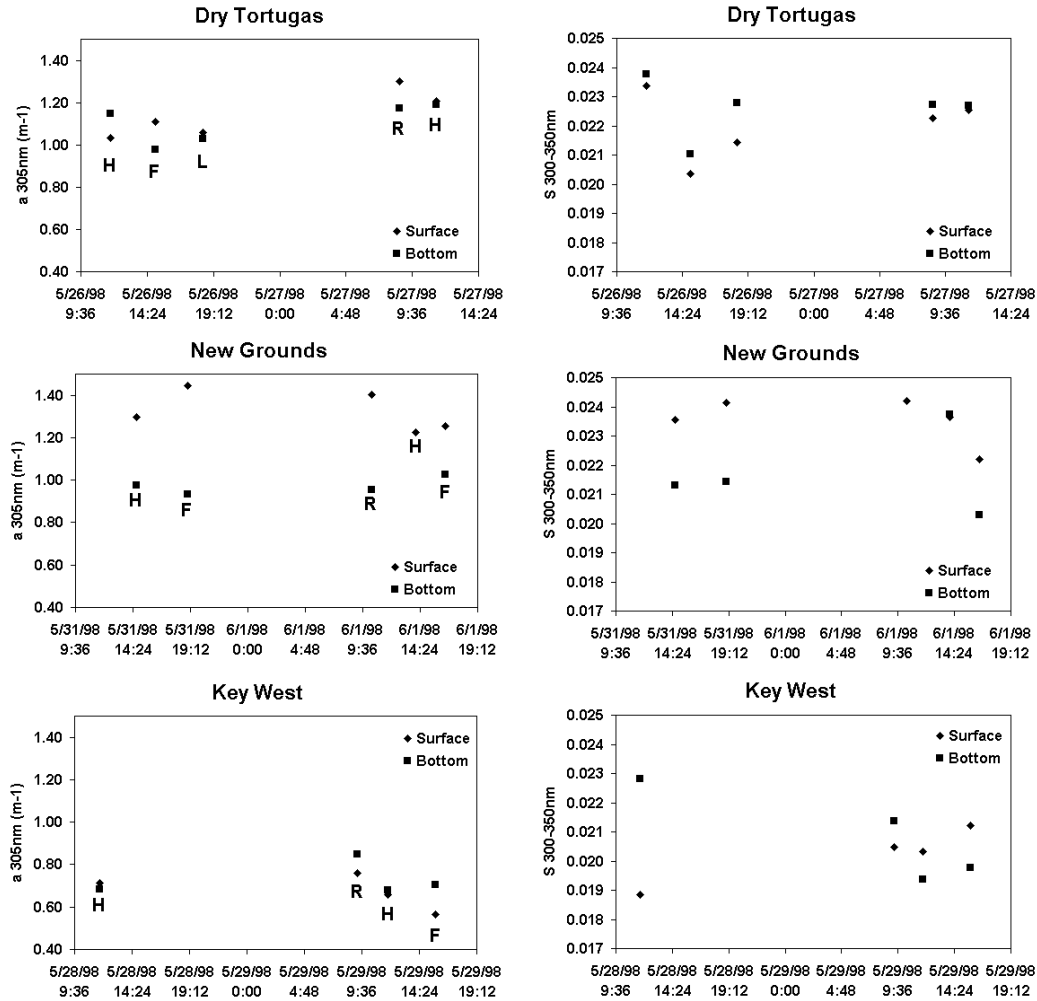
Figure 17: Tidal cycle a_{CDOM} 305nm and S(300-350nm) data collected on various reefs in the Florida Keys during the two cruises. Date and time are plotted on the x-axis. Tidal state is indicated by: H = high tide, F = falling tide, L = low tide and R = rising tide on the a_{CDOM} plots.
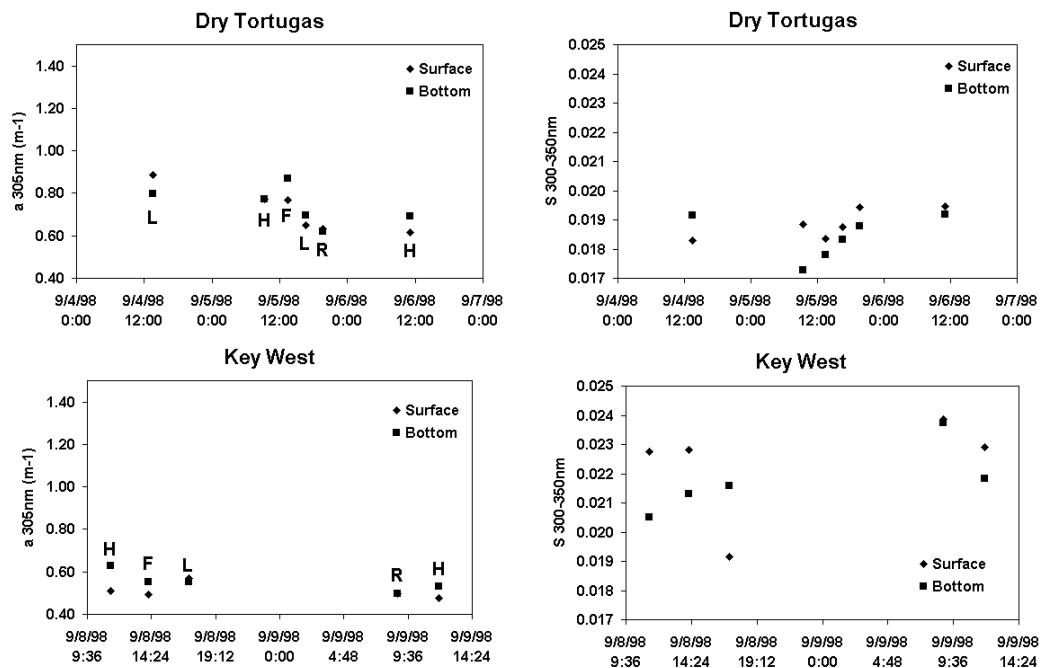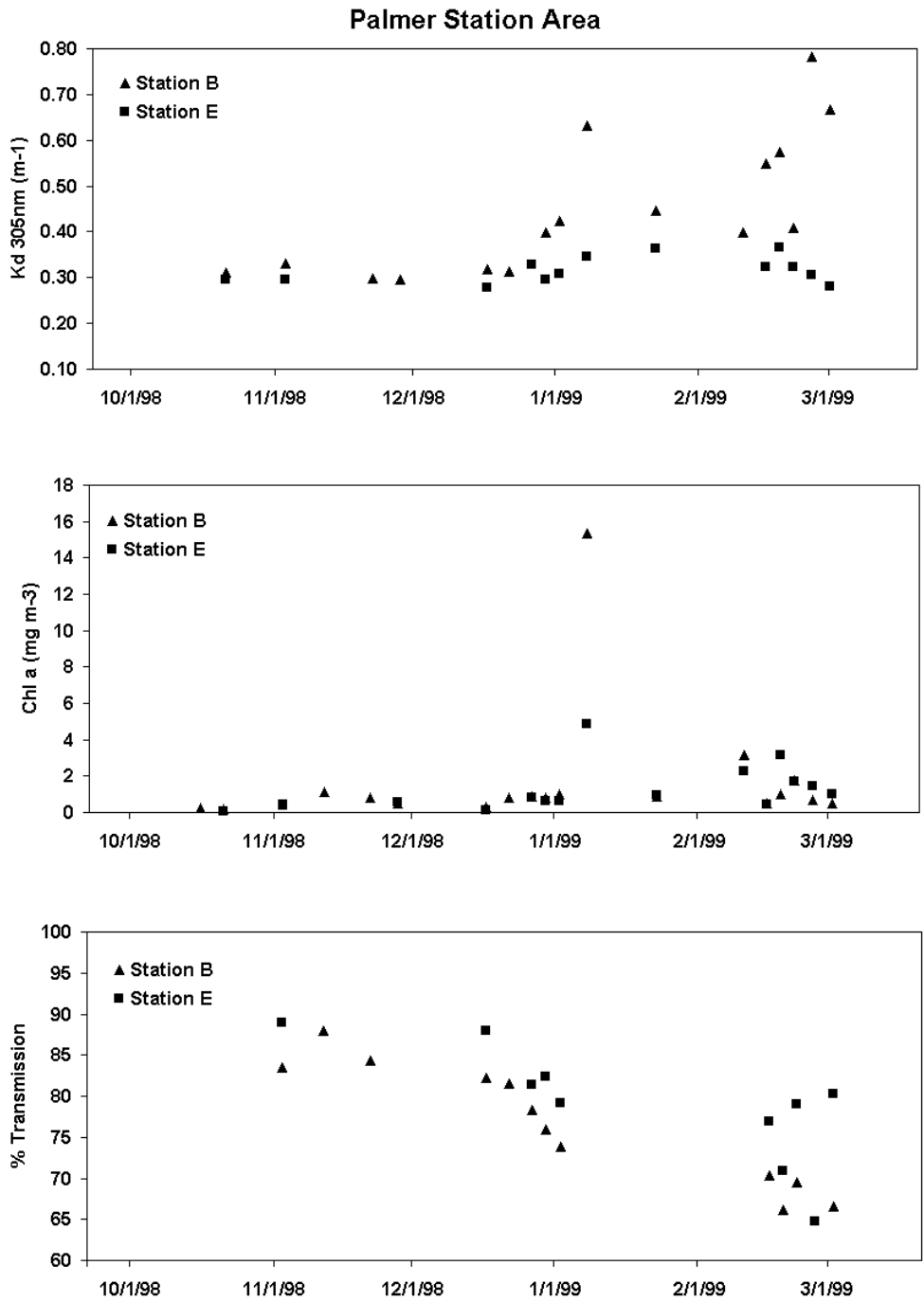
Figure 17: (continued)

Figure 18: Time series of UV attenuation at 305nm at stations B and E near Palmer Station, Antarctica. Time series of total surface chlorophyll *a* and percent transmission at 660nm from the CTD transmissometer are also plotted for comparison.

76

8. Summary and Conclusions

There is currently a need for algorithms estimating the penetration of UV radiation from visible optical measurements in seawater for use in estimating potential impacts of UV radiation on marine ecosystems. Currently, marine UV measurements are not standardized and there are often issues of compatibility between datasets collected using different instruments. Measuring UV attenuation in seawater is complicated further by low photon fluxes and rapid increases in the total UV attenuation coefficient with decreasing wavelength. Visible seawater measurements have become somewhat standardized to be compatible with SeaWiFS and other ocean color satellite measurements and have added advantages of higher photon fluxes and lower seawater attenuation, thus allowing measurements of these wavelengths to be made to much greater depths than the short UVB wavelengths.

In chapter 3, simple correlation relationships were established between UV attenuation coefficients and visible measurements for a wide variety of water compositions (Table 2). To first order, UV attenuation can be estimated from attenuation at 412nm. However, there were some special cases where this relationship must be used with caution. During times of very high particulate load, K(UV) could not be accurately calculated, thus caution should be taken in applying such algorithms during periods of very high particulate loads. Second, relationships between K(UV) and K(412) did not hold true for the Florida Keys – May 1998 cruise. In this case, a_{CDOM} overwhelmingly dominated K(UV) through both the UVB and UVA compared to the other regions (Figure 9). While relationships were found between K(UV) and K(412), similar relationships were not found for a_{CDOM}(UV) and K(412). Since the a_{CDOM} spectrum decreases

exponentially with increasing wavelength, detecting a_{CDOM} variability from measurements at 412nm, which is a wavelength highly absorbed by phytoplankton, is extremely difficult.

Also in chapter 3, the remote sensing reflectance ratio, $R_{rs}(555)/R_{rs}(412)$ showed especially notable utility for estimating K(UV). When estimating K(UV) from K(412), there were significant regional differences in the slopes of the linear fits to the data (Figures 6-7). These regional differences between the highly productive and highly variable waters of the Santa Barbara Channel and the generally low productivity, low a_{CDOM} waters of the west Antarctic Peninsula were minimized when $R_{rs}(555)/R_{rs}(412)$ was used to estimate K(UV) (Figure 8). Such utility of $R_{rs}(555)/R_{rs}(412)$ across regions was not expected as previous remote sensing reflectance waveband ratio algorithms have shown that regional algorithms are necessary for accurate estimation of chlorophyll in Antarctic waters due to low values of a_{CDOM} and terrestrially-derived particulates (Mitchell and Holm-Hansen, 1991; Ray Smith and Heidi Dierssen, personal communication). Since the PRR/PUV channels correspond to SeaWiFS satellite bands, the remote sensing reflectance ratio algorithms developed in Chapter 3 are directly applicable to SeaWiFS satellite data with corrections for transmission across the air-water interface and the earth's atmosphere.

As shown in chapter 4, there is a great deal of research that yet needs to be done before we can develop an accurate component model of UV attenuation in seawater for optical closure studies. First, there are very few published pure water absorption measurements in the 300-400nm wavelength range (Figure 10). All of these published pure water values have been questioned or disputed at some point in time. Second, there have been relatively few datasets published on natural particulate

78

attenuation in the ultraviolet. The UV absorption spectrum for natural phytoplankton communities can be highly variable in shape, since many common phytoplankton species have the ability to make UV-protective pigments (Karsten *et al.*, 1998; Karentz *et al.*, 1991; Dunlap *et al.*, 1995; Shick *et al.*, 1992; Vernet and Whitehead, 1996).

One area in which model parameters were improved in the ultraviolet is in the parameterization of UV absorption by chromophoric dissolved organic matter. In the past, a_{CDOM} has been parameterized by the absorption at a reference wavelength and the slope of a simple exponential curve fit. Wavelength ranges used to calculate the slope parameter (S) published in the literature can vary considerably. With the variability in a_{CDOM} values encountered during the studies presented, the wavelength at which a_{CDOM} became undetectable ranged between about 320-600nm. This wide range in the wavelength at which a_{CDOM} becomes undetectable spawned interest in assuring slope parameters calculated using different wavelength ranges were comparable to one another. As shown in Figure 11, the slope of the exponential curve fit is highly dependent on the wavelength interval used and the change in the slope parameter through the 300-400nm range can be approximated to first order as a linear function of wavelength. However, there is still a great deal of variability in the wavelength dependence of the slope parameter, which cannot yet be predicted or estimated, including absorption peaks or shoulders in the a_{CDOM} spectra (Figure 12).

As expected, a_{CDOM} was shown to dominate UVB attenuation in seawater, and a_{CDOM} dominance decreased as wavelength increased through the UVA (Figure 9, Table 3). The wide range of correlation coefficients shown on Figure 9 is evidence that a_{CDOM} cannot generally be assumed to maintain constant proportion with phytoplankton or total

particulate matter, which has been an assumption used in some models in the past (i.e. Tassan, 1994).

Analysis of spatial and temporal patterns of UV attenuation and a_{CDOM} parameters discussed in chapters 6 and 7 provided insight into the main influences on UV attenuation in each of the study regions. As expected, the transport of land-derived CDOM appears to have the largest impact on spatial and temporal patterns of K(UV) and a_{CDOM}. The highest UV attenuation values were obtained in the Santa Barbara Channel during a period of extreme storm-water runoff in February 1998 (Figures 5 & 16) and in the Florida Keys in May 1998 (Figure 14) where the origin of high a_{CDOM} waters appears to be the shelf just off the wetlands of the Florida Everglades based on AVHRR imagery. In contrast, UV attenuation and a_{CDOM} values were extremely low in the Antarctic (Figure 15), where there is minimal terrigenous influence.

While quantitative relationships could not be made, periods of high K(UV) and a_{CDOM} were also associated with phytoplankton bloom conditions in both the Santa Barbara Channel and in the Antarctic. Similar spatial patterns were found between chlorophyll *a* and K(UV) (or a_{CDOM}) during a few individual cruises in the Santa Barbara Channel, usually during time periods when storm activity was minimal. Looking at temporal variability in the Santa Barbara Channel, two of three peaks in K(UV) and a_{CDOM} could be attributed to phytoplankton blooms during upwelling conditions (Figure 16). The spatial variability observed during the January 1999 cruise in the Antarctic shows that areas of increased UV attenuation and a_{CDOM} values coincided with areas of increased primary productivity (Figure 15), with the highest values found in the southeast corner of the grid in the biologically dense surface waters of Marguerite Bay. Temporally, general trends in UV attenuation at station E in the Palmer

Station area closely match general trends in surface chlorophyll *a* (Figure 18). Temporal variability at station B also showed similarities to temporal variability in surface chlorophyll *a*, with the exception of the end of the season when there were significant quantities of glacial flour in the water (Figure 18).

While the major features can be attributed to either high inputs of terrigenous materials or phytoplankton blooms, smaller magnitude variations are much more difficult to explain, and for the most part cannot be explained or predicted using the data collected. However, variations in K(UV) and a_{CDOM} often correlated with surface seawater temperature (Figure 13 & 14), indicating changes in local currents, stratification and other physical processes may control, to some extent, UV attenuation at individual stations in these regions. Indeed, both the Santa Barbara Channel and Florida Keys study regions were located in areas where contrasting water masses interact in complex current regimes. Moderate correlations with sea surface temperature indicate that satellite MCSST (Multi-Channel Sea Surface Temperature) patterns may be of use in identifying relative patterns of UV attenuation in coastal waters. Unfortunately, quantitative correlations could not be determined using AVHRR MCSST images due to diurnal cycles of whole-region temperature shifts and the rarity of cloud-free images coinciding with sampling days.

The work presented provides algorithms which may be of great utility in initial modeling efforts to estimate the impact of UV radiation on coastal marine ecosystems from satellite imagery (Table 2). There is an interest in estimating the effects of UV radiation on coastal marine ecosystems, since changes in seawater UV due to either changes in atmospheric ozone, patterns of cloud cover, or changes in the transparency of the local waters may significantly impact photochemical

and photobiological processes important to global carbon cycling and trophic-level interactions (reviewed in Häder *et al.*, 1995; Zepp *et al.*, 1995, Häder and Worrest, 1991; Bothwell *et al.*, 1994).   However, as noted in chapter 4, we are still only in the beginning stages of collecting quality data sets for use in developing quality optical closure models for the UV portion of the solar spectrum.

9. References

(1992) *PUV-500 Profiling Ultraviolet Radiometer user's manual.* Biospherical Instruments, Inc., San Diego, CA 92110.

Austin, R. W. (1974) Inherent spectral radiance signatures of the ocean surface. In: *Ocean Color Analysis.* S. W. Duntley, R. W. Austin, W. H. Wilson, C. F. Edgerton and S. E. Moran, editors. UCSD-SIO reference 74-10. pp. 1 – 20.

Baker, K. S. and R. C. Smith. (1982) Bio-optical classification and model of natural waters. 2. *Limnology and Oceanography* **27(3)**: 500 – 509.

Boivin, L. P., W. F. Davidson, R. S. Storey, D. Sinclair and E. D. Earle. (1986) Determination of the attenuation coefficients of visible and ultraviolet radiation in heavy water. *Applied Optics* **25(6)**: 877 – 882.

Bothwell, M. L., D. M. J. Sherbot and C. M. Pollock. (1994) Ecosystem response to solar ultraviolet-B radiation: Influence of trophic-level interactions. *Science* **265(5168)**: 97 – 100.

Bricaud, A., A. Morel and L. Prieur. (1981) Absorption by dissolved organic matter of the sea (yellow substance) in the UV and visible domains. *Limnology and Oceanography* **26(1)**: 43 – 53.

Buiteveld, H. (1994) The optical properties of pure water. *Ocean Optics XII* SPIE **2258**: 174 – 183.

Carder, K. L., R. G. Steward, G. R. Harvey and P. B. Ortner. (1989) Marine humic and fulvic acids: Their effects on remote sensing of ocean chlorophyll. *Limnology and Oceanography* **34(1)**: 68 – 81.

Cullen, J. J., P. J. Neale and M. P. Lesser. (1992) Biological weighting function for the inhibition of phytoplankton photosynthesis by ultraviolet radiation. *Science* **258(5082)**: 646 – 650.

Dunlap, W. C., G. A. Rae, E. W. Helbling, V. E. Villafañe and O. Holm-Hansen. (1995) Ultraviolet-absorbing compounds in natural assemblages of antarctic phytoplankton. *Antarctic Journal of the United States* **30**: 323 – 326.

Dütsch, H. U. and J. Staehelin. (1989) Discussion of the 60 year total ozone record at Arosa based on measurements of the vertical distribution and a meteorological parameter. *Planetary and Space Science* **37(12)**: 1587 – 1599.

Gleason, D. F. (1993) Differential effects of ultraviolet radiation on green and brown morphs of the Caribbean coral Porites astreoides. *Limnology and Oceanography* **38(7)**: 1452 – 1463.

Gleason, D. F. and G. W. Wellington. (1993) Ultraviolet radiation and coral bleaching. *Nature* **365**: 936 – 838.

Goreau, T. J. and R. L. Hayes. (1994) Coral bleaching and ocean hot spots. *Ambio* **23(3)**: 176-180.

Green, S. A. and N. V. Blough. (1994) Optical absorption and fluorescence properties of chromophoric dissolved organic matter in natural waters. *Limnology and Oceanography* **39(8)**: 1903 – 1916.

Häder, D.-P. and R. C. Worrest. (1991) Effects of enhanced solar ultraviolet radiation on aquatic ecosystems. *Photochemistry and Photobiology* **53(5)**: 717 – 725.

Häder, D.-P., R. C. Worrest, H. D. Kumar and R. C. Smith. (1995) Effects of increased solar ultraviolet radiation on aquatic ecosystems. *Ambio* **24(3)**: 174 – 180.

Harms, S. and C. D. Winant. (1998) Characteristic patterns of the circulation in the Santa Barbara Channel. *Journal of Geophysical Research* **103(2)**: 3041 – 3065.

Hendershott, M. C. and C. D. Winant. (1996) Surface circulation in the Santa Barbara Channel. *Oceanography* **9(2)**: 114 – 121.

Herman, J. R., P. K. Bhartia, J. Ziemke, Z. Ahmad and D. Larko. (1996) UV-B increases (1979-1992) from decreases in total ozone. *Geophysical Research Letters* **23(16)**: 2117 – 2120.

Hoegh-Guldberg, O. and G. J. Smith. (1989) The effect of sudden changes in temperature, light and salinity on the population density and export of zooxanthellae from the reef corals *Stylophora pistillata* Esper and *Seriatopora hystrix* Dana. *Journal of Experimental Marine Biology and Ecology* **129(3)**: 279 – 303.

Hoge, F. E., M. E. Williams, R. N. Swift, J. K. Yungel and A. Vodacek. (1995) Satellite retrieval of the absorption coefficient of chromophoric dissolved organic matter in continental margins. *Journal of Geophysical Research* **100(12)**: 24847 – 24854.

Hornafius, J. S., D. Quigley and B. P. Luyendyk. (1999) The world's most spectacular marine hydrocarbon seeps (Coal Oil Point, Santa Barbara Channel, California): Quantification of emissions. *Journal of Geophysical Research* **104(9)**: 20703 – 20711.

Hughes, T. P. and J. H. Connell. (1999) Multiple stressors on coral reefs: A long-term perspective. *Limnology and Oceanography* **44(3, part 2)**: 932 – 940.

Hunter, J. R., S. E. Kaupp and J. H. Taylor. (1982) Assessment of effects of UV radiation on marine fish larvae. *The Role of Solar Ultraviolet Radiation in Marine Ecosystems.* J. Calkins, editor. New York. 459 – 497.

Hunter, J. R., S. E. Kaupp and J. H. Taylor. (1981) Effects of solar and artificial ultraviolet-B radiation on larval northern anchovy, *Engraulis mordax. Photochemistry and Photobiology* **34**: 477 – 486.

Jones, L. W. and B. Kok. (1966) Photoinhibition of chloroplast reactions. 1. Kinetics and action spectra. *Plant Physiology* **41**: 1037 – 1043.

Karentz, D. F. S. McEuen, M. C. Land and W. C. Dunlap. (1991) Survey of mycosporine-like amino acid compounds in Antarctic marine organisms: potential protection from ultraviolet exposure. *Marine Biology* **108**: 157 – 166.

Karsten, U. T. Sawall, D. Hanelt, K. Bischof, F. L. Figueroa, A. Flores-Moya and C. Wiencke. (1998) An inventory of UV-absorbing mycosporine-like amino acids in macroalgae from polar to warm-temperate regions. *Botanica Marina* **41**: 443 – 453.

Kinzie, R. A., III. (1993) Effects of ambient levels of solar ultraviolet radiation on zooxanthellae and photosynthesis of the reef coral *Montipora verrucosa. Marine Biology* **116**: 319 – 327.

Kirk, J. T. O. (1994a) Optics of UV-B radiation in natural waters. *Ergebnisse der Limnologie.* **43**: 1 – 16.

Kirk, J. T. O. (1994b) *Light and Photosynthesis in Aquatic Ecosystems.* Second Edition. Cambridge University Press. New York.

Klimkin, V. M., V. G. Sokovikov and V. N. Fedorishchev. (1993) Spectrofluorimeter for remote analysis of oils on water surface. *Optical Monitoring of the Environment.* N. N. Belov and E. I. Akopov editors. SPIE. Bellingham, WA. **2107**: 218 – 231.

Kouassi, A. M. and R. G. Zika. (1992) Light-induced destruction of the absorbance property of dissolved organic matter in seawater. *Toxicological and Environmental Chemistry* **35(3-4)**: 195 – 211.

Lenarz, W. H., D. A. VenTresca, W. M. Graham, F. B. Schwing and F. Chavez. (1995) Explorations of El Niño events and associated biological population dynamics off central California. *California*

Cooperative Oceanic Fisheries Investigations Reports **36**: 106 – 119.

Lesser, M. P., W. R. Stochaj, D. W. Tapley and J. M. Shick. (1990) Bleaching in coral reef anthozoans: Effects of irradiance, ultraviolet radiation, and temperature on the activities of protective enzymes against active oxygen. *Coral Reefs* **8(4)**: 225 – 232.

Lindell, M. J., G. Wilhelm and L. J. Tranvik. (1995) Enhanced bacterial growth in response to photochemical transformation of dissolved organic matter. *Limnology and Oceanography* **40(1)**: 195 – 199.

Lee, T. N., M. E. Clarke, E. Williams, A. F. Szmant and T. Berger. (1994) Evolution of the Tortugas gyre and its influence on recruitment in the Florida Keys. *Bulletin of Marine Science* **54(3)**: 621 – 646.

Litjens, R. A. J., T. I. Quickenden and C. G. Freeman. (1999) Visible and near-ultraviolet absorption spectrum of liquid water. *Applied Optics* **38(7)**: 1216 – 1223.

Lubin, D. and J. E. Frederick. (1991) The ultraviolet radiation environment of the Antarctic Peninsula: The roles of ozone and cloud cover. *Journal of Applied Meteorology* **30(4)**: 478 – 493.

McPeters, R. D., S. M. Hollandsworth, L. E. Flynn, J. R. Herman, C. J. Seftor. (1996) Long-term ozone trends derived from the 16-year combined Nimbus 7/Meteor 3 TOMS Version 7 record. *Geophysical Research Letters* **23(25)**: 3699 – 3702.

Mertes, L. A. K., M. Hickman, B. Waltenberger, A. L. Bortman, E. Inlander, C. McKenzie and J. Dvorsky. (1998) Synoptic views of sediment plumes and coastal geography of the Santa Barbara Channel, California. *Hydrological Processes* **12(6)**: 967 – 979.

Miller, W. L. and M. A. Moran. (1997) Interaction of photochemical and microbial processes in the degradation of refractory dissolved

organic matter from a coastal marine environment. *Limnology and Oceanography* **42(6)**: 1317 – 1324.

Mitchell, B. G. and O. Holm-Hansen. (1991) Bio-optical properties of Antarctic Peninsula waters: differentiation from temperate ocean models. *Deep-Sea Research* **38(8-9)**: 1009 – 1028.

Mobley, C. D. (1994) *Light and Water: Radiative Transfer in Natural Waters.* Academic Press. San Diego.

Molina, L. T. and M. J. Molina. (1986) Absolute absorption cross sections of ozone in the 185- to 350-nm wavelength range. *Journal of Geophysical Research* **91**: 14501 – 14508.

Mopper, K., R. S. Sarpal, D. J. Kieber. (1995) Protein and humic substance fluorescence of dissolved organic matter in antarctic sea water. *Antarctic Journal of the United States* **30(5)**: 127 – 139.

Moran, M. A. and R. G. Zepp. (1997) Role of photoreactions in the formation of biologically labile compounds from dissolved organic matter. *Limnology and Oceanography* **42(6)**: 1307 – 1316.

Murphree, T. and C. Reynolds. (1995) El Niño and La Niña effects on the northeast Pacific: The 1991 – 1993 and 1988 – 1989 events. *California Cooperative Oceanic Fisheries Investigations Reports* **36**: 45 – 56.

O'Reilly, J. E., S. Maritorena, B. G. Mitchell, D. A. Siegel, K. L. Carder, S. A. Garver, M. Kahru and C. McClain. (1998) Ocean color chlorophyll algorithms for SeaWiFS. *Journal of Geophysical Research* **103(11)**: 24937 – 24953.

Pares-Sierra, A. and J. J. O'Brien. (1989) The seasonal and interannual variability of the California Current system: A numerical model. *Journal of Geophysical Research* **94(3)**: 3159 – 3180.

Patterson, K. W. (1996) *Calculation of biologically effective UV dose rates for larval anchovies in the Southern California Bight using PUV data in combination with a simple high-spectral resolution model.* Master's Thesis. University of California, Santa Barbara.

Patterson, K. W., R. C. Smith and C. R. Booth. (1996) A method for removing a majority of the error in PUV attenuation coefficients due to spectral drift in response with depth in the water column. *Ocean Optics XIII* SPIE **2963**: 737 – 742.

Pope, R. M. and E. S. Fry. (1997) Absorption spectrum (380-700 nm) of pure water. II. Integrating cavity measurements. *Applied Optics* **36(33)**: 8710 – 8723.

Porter, J. W., S. K. Lewis and K. G. Porter. (1999) The effect of multiple stressors on the Florida Keys coral reef ecosystem: A landscape hypothesis and a physiological test. *Limnology and Oceanography* **44(3, part 2)**: 941 – 949.

Preisendorfer, R. W. (1961) Application of radiative transfer theory to light measurements in the sea. *Union Geod. Geophys. Inst. Monogr.* **10**: 11 – 30.

Quickenden, T. I. and J. A. Irvin. (1980) The ultraviolet absorption spectrum of liquid water. *Journal of Chemical Physics* **72(8)**: 4416 – 4428.

Setlow, R. (1974) The wavelengths in sunlight effective in producing skin cancer: a theoretical analysis. *Proceedings of the National Academy of Science, U. S. A.* **71**: 3363 – 3366.

Shick, J. M., W. C. Dunlap, B. E. Chalker, A. T. Banaszak and T. K. Rosenzsweig. (1992) Survey of ultraviolet radiation-absorbing mycosporine-like amino acids in organs of coral reef holothuriods. *Marine Ecology Progress Series* **90(2)**: 139 – 148.

Smith, R. C., K. S. Baker, W. R. Fraser, E. E. Hofmann, D. M. Karl, J. M. Klinck, L. B. Quetin, B. B. Prézelin, R. M. Ross, W. Z. Trivelpiece and M. Vernet. (1995) The Palmer LTER: A long-term ecological research program at Palmer Station, Antarctica. *Oceanography* **8(3)**: 77 – 86.

Smith, R. C., H. M. Dierssen and M. Vernet. (1996) Phytoplankton biomass and productivity in the western Antarctic Peninsula region. *Foundations for Ecological Research West of the Antarctic Peninsula. Antarctic Research Series* **70**: 333 – 356.

Smith, R. C., Z. M. Wan and K. S. Baker. (1992) Ozone depletion in Antarctica – modeling its effect on solar UV irradiance under clear-sky conditions. *Journal of Geophysical Research* **97**: 7383 – 7397.

Smith, R. C. and K. S. Baker. (1981) Optical properties of the clearest natural waters (200-800 nm). *Applied Optics* **20(2)**: 177 – 184.

Sogandares, F. M. and E. S. Fry. (1997) Absorption spectrum (340-640 nm) of pure water. I. Photothermal measurements. *Applied Optics* **36(33)**: 8699 – 8709.

Tassan, S. (1994) Local algorithms using SeaWiFS data for the retrieval of phytoplankton, pigments, suspended sediment, and yellow substance in coastal waters. *Applied Optics* **33(12)**: 2369 – 2378.

Venrick, E. L. (1998) The phytoplankton of the Santa Barbara Basin: Patterns of chlorophyll and species structure and their relationships with those of surrounding stations. *California Cooperative Oceanic Fisheries Investigations Reports* **39**: 124 – 132.

Vernet, M. and K. Whitehead. (1996) Release of ultraviolet-absorbing compounds by the red-tide dinoflagellate *Lingulodinium polyedra*. *Marine Biology* **127**: 35 – 44.

Vetter, R. D., A. Kurtzman and T. Mori. (1999) Diel cycles of DNA damage and repair in eggs and larvae of northern anchovy, *Engraulis mordax*, exposed to solar ultraviolet radiation. *Photochemistry and Photobiology* **69(1)**: 27 – 33.

Vodacek, A., N. V. Blough, M. D. DeGrandpre, E. T. Peltzer and R. K. Nelson. (1997) Seasonal variation of CDOM and DOC in the Middle Atlantic Bight: Terrestrial inputs and photooxidation. *Limnology and Oceanography* **42(4)**: 674 – 686.

Waters, K. J., R. C. Smith and M. R. Lewis. (1990) Avoiding ship-induced light-field perturbation in the determination of oceanic optical properties. *Oceanography* **3**: 18 – 21.

Zepp, R. G., T. Callaghan and D. Erickson. (1995) Effects of increased solar ultraviolet radiation on biogeochemical cycles. *Ambio* **24(3)**: 181 – 187.

Zepp, R. G. and P. F. Schlotzhauer. (1981) Comparison of photochemical behavior of various humic substances in water: III. Spectroscopic properties of humic substances. *Chemosphere* **10(5)**: 479 – 486.